Results Math 72 (2017), 1281–1313

1422-6383/17/031281-33
published online February 27, 2017
DOI 10.1007/s00025-017-0659-7

Results in Mathematics

Shape-Adjustable Generalized Bézier Rotation Surfaces with Multiple Shape Parameters

Gang Hu, Guo Wei, and Junli Wu

Abstract. To tackle the problems in adjusting and controlling shapes of rotation surfaces, a new efficient method for quickly constructing generalized Bézier rotation surfaces with multiple shape parameters is proposed. Firstly, following the important idea of transfinite vectored rational interpolating function, the shape-adjustable generalized Bézier rotation surfaces are constructed using a generalized Bézier curve with multiple shape parameters. Secondly, the explicit function expression of the shape-adjustable generalized Bézier rotation surfaces is presented. The new rotation surfaces inherit the outstanding properties of the Bézier rotation surfaces, with a good performance on adjusting their local shapes by changing the shape parameters. Finally, some properties of the new rotation surfaces are discussed, and the influence rules of the shape parameters on the new rotation surfaces are studied. The modeling examples illustrate that the shape-adjustable generalized Bézier rotation surfaces provide a valuable way for the design of rotation surfaces.

Mathematics Subject Classification. 65D07, 65D10, 65D17, 65D18, 68U05, 68U07.

Keywords. Rotation surface, Generalized Bézier curves, Shape parameter, Transfinite vectored rational interpolating function.

1. Introduction

Rotation surface is a kind of special and common geometric profile. The geometric shapes of many objects are rotation surfaces in nature and the field of product modeling design. A rotation surface is usually generated by rotating a curve with a fixed angle around a straight line in space. Being a kind of special

and significant one, rotation surface has very extensive applications in many areas, such as aerospace, architectural design, machining, industrial design and computer graphics. For instance, due to the fact that the surface models of many objects are composed of rotation surfaces or sequences of rotation surfaces that are connected end to end, the problems about the generation and explicit function expression of rotation surfaces are involved in the design or manufacturing of many products like auto bodies, airplane skins, ship hulls, moulds, fine-art objects, and the field of 3D cartoon and architecture [1,2]. Now, how to effectively and quickly obtain the 3D mathematical models of rotation surfaces has been an important research content in computer aided geometric design and computer graphics, while rotation surfaces are still usually expressed in Bézier parametric form in current CAD/CAM system. Therefore, the research on Bézier rotation surfaces has very significant theoretical and practical application value.

Given the importance of rotation surfaces, scholars at home and abroad have carried out extensive research on how to construct rotation surfaces and have obtained some significant results [3–16]. At present, the methods for designing rotation surfaces can be divided into the following three broad categories: the rotation surfaces represented by free surfaces, the coordinate transformation method and the methods for generating special rotation surfaces. The rotation surface representation based on free surfaces often exactly represent a rotation surface by using a kind of parametric surface (such as Rational Bézier Surface, Rational B-Spline Surface, NURBS Surface, C-B-Spline Surface and T-B-Spline Surface) [3–7]. For example, Farin et al. [3], Wang [4], Kang et al. [5] gave the necessary and sufficient conditions for representing rotation surfaces by rational Bézier surfaces, quadric rational B-Spline surfaces and NURBS surfaces respectively. Meanwhile they derived the corresponding constraint equations that the control points and weight factors of the surface they studied need to satisfy for representing a rotation surface. Zeng and Ma et al. studied the modeling technology of using C-B-Spline Surfaces and T-B-Spline Surfaces to construct rotation surfaces in [6,7], respectively. In addition, each of them gave his own specific calculating method for generating rotation surfaces. However, a common problem of the rotation surfaces generated by these free surfaces is that it will be very troublesome to readjust the shapes of these rotation surfaces, that is, if the shape of a rotation surface need to be modified, it is necessary to recalculate its control points and weight factors according to the corresponding constraint equations, which makes the operation cumbersome and computation complex and will inconvenience designers in appearance design. The main idea of the coordinate transformation method [1,8,19] is that, given a parametric curve $\boldsymbol{l}(t)$ in space as the generating line and a straight line $\boldsymbol{L}(t)$ as the rotation axis, a rotation surface can be constructed by rotating the generating line $\boldsymbol{l}(t)$ with a fixed angle $\theta(0 < \theta \leq 2\pi)$ around the rotation axis $\boldsymbol{L}(t)$. Moreover, the equation of the rotation surface can be obtained by using 3D rotation transformation. For instance, assuming

that the generating line $\boldsymbol{l}(t)$ is a parametric curve in the plane xoz (noting: the parametric curve can also be a free curve, such as Bézier, B-Spline and NURBS curve et. al) and the rotation axis $\boldsymbol{L}(t)$ is the z axis, then the equation of the rotation surface $\boldsymbol{S}$ can be expressed as follows [8,19]:

$$\boldsymbol{S}(t,\theta) = \begin{pmatrix} \cos\theta & -\sin\theta & 0 \\ \sin\theta & \cos\theta & 0 \\ 0 & 0 & 1 \end{pmatrix} \boldsymbol{l}(t) = [x(t)\cos\theta, x(t)\sin\theta, z(t)]^{\mathrm{T}}$$

where $0 < \theta \leq 2\pi$, the generating line $\boldsymbol{l}(t) = [x(t), 0, z(t)]^{\mathrm{T}}$, $t \in [t_0, t_1]$.

Similarly, the same problem exists in modifying the shape of this kind of rotation surface generated by the coordinate transformation method, that is, it is necessary to modify the generating line $\boldsymbol{l}(t)$ to readjust the shape of the rotation surface, which makes the design process take more time and energy. Besides, the equation of this kind of rotation surface contains trigonometric functions, which will increase the computation complexity and truncation error in constructing a rotation surface. The methods for generating special rotation surfaces are proposed to construct the rotation surfaces with specific characteristics (or in order to achieve some particular purpose). The typical works of these methods are drawing of rotation surfaces for illustration and annotation in 3D [9], generalized revolving surface based on metamorphose curve [10], free form modeling with variational implicit surfaces [11], 3D reconstruction of rotation surfaces [12–14], generation and shape adjustment of revolution surface based on stream curve [15], rotation surface modeling technique by cubic B-spline free drawing [16], continuous forming for rotary surface based on multi-point adjusting principle [17], subdivision method of revolution surfaces [18] and blends between quadrics of revolution [19], etc. Though each of these special rotation surfaces generated in [4,8–13,15–17,19] has its own significant improvements, the applicable ranges of them have certain limitations and they also have many other drawbacks, such as the limitation of shape adjustability, the lack of explicit expression and calculation complexity, etc.

In practical applications, designers often need to adjust the partial or whole shape of a rotating surface intuitively and handily, so the research on how to quickly generate special rotation surfaces which are easy for shape analysis and adjustment has certain practical significance. Thus, we construct a family of shape-adjustable generalized Bézier curves, combined with the theory of transfinite vectored rational interpolating function, and then we study the generating technology of shape-adjustable generalized Bézier rotation surfaces, by which many rotation surfaces in different shapes can be constructed. What's more, we can modify the shapes of these rotation surfaces globally or locally, further enhancing their shape adjustability.

The remainder of the paper is organized as follows. The definition and continuity condition of shape-adjustable generalized Bézier curves are given in Sect. 2. In Sect. 3, we describe the transfinite vector valued rational interpolation function. A novel algorithm for constructing a shape-adjustable

generalized Bézier rotation surfaces is given in Sect. 4. In Sect. 5, some practical examples are given and we present some practical applications. At last, some conclusions are given in Sect. 6.

2. A Family of Shape-Adjustable Generalized Bézier Curves

2.1. Definition of Shape-Adjustable Generalized Bézier Curves

Similar to the construction of Bézier curves, given a set of control points $\boldsymbol{P}_i \in \mathrm{R}^u$ $(u = 2, 3; i = 0, 1, 2, 3)$ located in a plane or space, a family of parametric curves $\{\hat{\prod}_t\}$ can be defined, whose equation in matrix form is expressed as follows:

$$\left\{\hat{\prod}_t\right\} : \ \boldsymbol{L}(t; \lambda_1, \lambda_2, \lambda_3, \omega) = \boldsymbol{TMP}^{\mathrm{T}}, \quad 0 \le t \le 1 \tag{1}$$

where $\boldsymbol{T} = [t^4, t^3, t^2, t, 1], \boldsymbol{P} = [\boldsymbol{P}_0, \boldsymbol{P}_1, \boldsymbol{P}_2, \boldsymbol{P}_3]$.

$$\boldsymbol{M} = \begin{pmatrix} -\lambda_1\omega + \omega & \lambda_1\omega + \lambda_2\omega - 4\omega & \lambda_3\omega - \lambda_2\omega + 2\omega & -\lambda_3\omega + \omega \\ 3\lambda_1\omega - 3\omega - 1 & 9\omega - 3\lambda_1\omega - 2\lambda_2\omega + 3 & -5\omega + 2\lambda_2\omega - \lambda_3\omega - 3 & 1 + \lambda_3\omega - \omega \\ 3 - 3\lambda_1\omega + 3\omega & -6 - 6\omega + 3\lambda_1\omega + \lambda_2\omega & 3 + 3\omega - \lambda_2\omega & 0 \\ \lambda_1\omega - \omega - 3 & 3 + \omega - \lambda_1\omega & 0 & 0 \\ 1 & 0 & 0 & 0 \end{pmatrix}$$

here $\lambda_1, \lambda_3 \in [0, 4], \lambda_2 \in [0, 6]$ and $\omega \in [0, 1]$ are local or global shape parameters of the curve.

In this paper, the curve defined by (1) is called a shape-adjustable generalized Bézier (or SG-Bézier, for short) curve. Given the four control points $\boldsymbol{P}_0, \boldsymbol{P}_1, \boldsymbol{P}_2, \boldsymbol{P}_3$, then a family of SG-Bézier curves can be generated by (1) when each of the shape parameters $\lambda_i (i = 1, 2, 3)$ and ω varies during its value range. It can be easily proved that the SG-Bézier curves inherit most outstanding properties of the traditional Bézier curves, such as convex hull properties, symmetry, terminal properties, affine invariance and variation diminishing property. Furthermore, due to the fact that the curve defined by (1) has four shape parameters, we have 3^4-1 different ways to modify its local or global shape flexibly under the condition that its control points remain unchanged. In particular, when $\omega = 0$ or $\lambda_1 = \lambda_3 = 1, \lambda_2 = 3$, the curve will degrade into the traditional cubic Bézier curve. Figure 1 shows graphs of SG-Bézier curves with the same control polygon and different shape parameters. Figure 1a shows the generated curve with $\omega = 1, 0.75, 0.5, 0.25, 0$ and $\lambda_i (i = 1, 2, 3)$ remaining unchanged from bottom to top; Fig. 1b shows the generated curve with $\lambda_1 = 4, 3, 2, 1, 0$ and $\omega, \lambda_2, \lambda_3$ remaining unchanged from bottom to top; Fig. 1c shows the generated curve with $\lambda_2 = 6, 4.5, 3, 1.5, 0$ and $\omega, \lambda_1, \lambda_3$ remaining unchanged from bottom to top; Fig. 1d shows the generated curve with $\lambda_3 = 4, 3, 2, 1, 0$ and $\omega, \lambda_1, \lambda_2$ remaining unchanged from bottom to top. Figure 1 intuitively reveals that the larger the shape parameter ω,

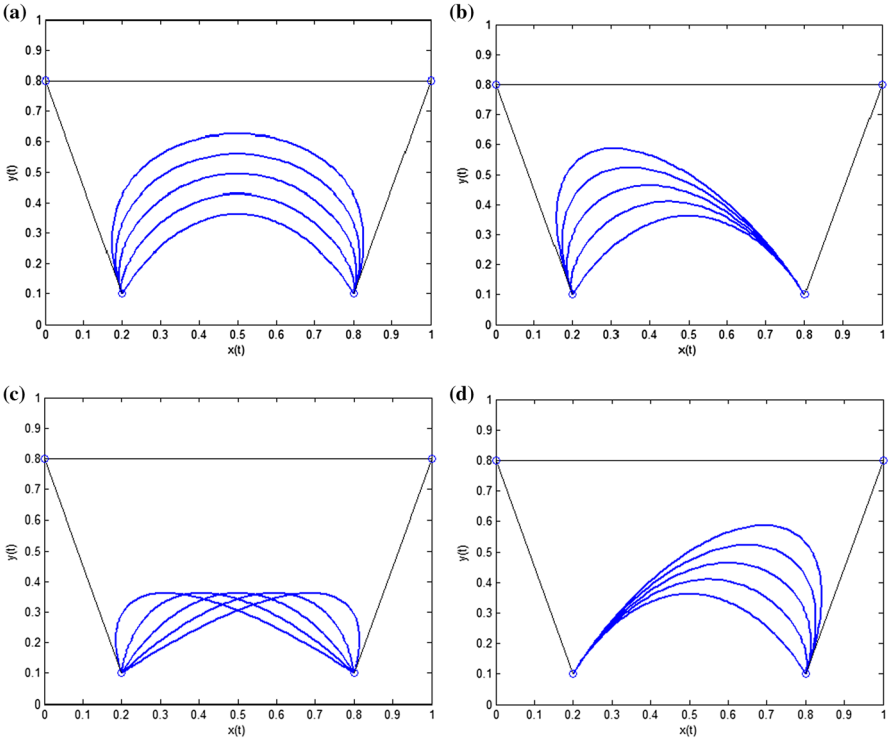

FIGURE 1. SG-Bézier curves with the same control polygon and different shape parameters. **a** $\lambda_1 = 4, \lambda_2 = 3, \lambda_3 = 4; \omega = 1, 0.75, 0.5, 0.25, 0;$ **b** $\omega = 1, \lambda_2 = 3, \lambda_3 = 4; \lambda_1 = 4, 3, 2, 1, 0;$. **c** $\lambda_1 = 4, \omega = 1, \lambda_3 = 4; \lambda_2 = 6, 4.5, 3, 1.5, 0;$ **d** $\lambda_1 = 4, \lambda_2 = 3, \omega = 1; \lambda_3 = 4, 3, 2, 1, 0;$

the farther away the curve moves from its control polygon. So the shape parameter ω can modify the global shape of a curve, while the shape parameters $\lambda_1, \lambda_2, \lambda_3$ realize the local change of the curve's shape.

2.2. Continuity Condition of Shape-Adjustable Generalized Bézier Curves

As it is difficult to construct a complex curve by a single SG-Bézier curve, the key technology need to be solved is to realize the smooth continuity between SG-Bézier curves. Similar to the smooth continuity between traditional Bézier curves, the following conclusions about the smooth continuity conditions for SG-Bézier curves can be derived.

Theorem 1. *The sufficient and necessary conditions for G^1 continuity between two SG-Bézier curves $\boldsymbol{L}_1(t; \lambda_{1,1}, \lambda_{2,1}, \lambda_{3,1}, \omega_1)$ and $\boldsymbol{L}_2(t; \lambda_{1,2}, \lambda_{2,2}, \lambda_{3,2}, \omega_2)$ at the joint are*

$$\begin{cases} \boldsymbol{P}_{0,2} = \boldsymbol{P}_{3,1} \\ \boldsymbol{P}_{1,2} = \left[1 + \frac{3+\omega_1-\omega_1\lambda_{3,1}}{\alpha(3+\omega_2-\omega_2\lambda_{1,2})}\right] \boldsymbol{P}_{3,1} - \frac{3+\omega_1-\omega_1\lambda_{3,1}}{\alpha(3+\omega_2-\omega_2\lambda_{1,2})} \boldsymbol{P}_{2,1} \end{cases} \tag{2}$$

where $\alpha > 0$ *is constant,* $\lambda_{i,j}, \omega_j (i = 1, 2, 3; j = 1, 2)$ *are shape parameters,* $\boldsymbol{P}_{i,1} (i = 0, 1, 2, 3)$ *and* $\boldsymbol{P}_{i,2} (i = 0, 1, 2, 3)$ *are control points of the SG-Bézier curves* $\boldsymbol{L}_1(t; \lambda_{1,1}, \lambda_{2,1}, \lambda_{3,1}, \omega_1)$ *and* $\boldsymbol{L}_2(t; \lambda_{1,2}, \lambda_{2,2}, \lambda_{3,2}, \omega_2)$*, respectively.*

Proof. If $\boldsymbol{L}_1(t; \lambda_{1,1}, \lambda_{2,1}, \lambda_{3,1}, \omega_1)$ and $\boldsymbol{L}_2(t; \lambda_{1,2}, \lambda_{2,2}, \lambda_{3,2}, \omega_2)$ need to achieve the G^1 continuity, it is necessary that they achieve the G^0 continuity at the joint first, which means

$$\boldsymbol{L}_1(1; \lambda_{1,1}, \lambda_{2,1}, \lambda_{3,1}, \omega_1) = \boldsymbol{L}_2(0; \lambda_{1,2}, \lambda_{2,2}, \lambda_{3,2}, \omega_2) \tag{3}$$

According to (1), the two curves meet the following conditions when $t = 1$ and $t = 0$

$$\begin{cases} \boldsymbol{L}_1(1; \lambda_{1,1}, \lambda_{2,1}, \lambda_{3,1}) = \boldsymbol{P}_{3,1} \\ \boldsymbol{L}_2(0; \lambda_{1,2}, \lambda_{2,2}, \lambda_{3,2}) = \boldsymbol{P}_{0,2} \end{cases} \tag{4}$$

Substituting (4) in (3), we have

$$\boldsymbol{P}_{0,2} = \boldsymbol{P}_{3,1} \tag{5}$$

The above Eq. (5) indicates that the first requirement for G^1 smooth continuity between the two curves is a common control point. □

In addition, the tangent vectors of the two curves need to satisfy the following condition

$$\boldsymbol{L}'_1(1; \lambda_{1,1}, \lambda_{2,1}, \lambda_{3,1}, \omega_1) = \alpha \boldsymbol{L}'_2(0; \lambda_{1,2}, \lambda_{2,2}, \lambda_{3,2}, \omega_2) \quad (\alpha > 0) \tag{6}$$

Then according to (1), we can obtain

$$\begin{cases} \boldsymbol{L}'_1(1; \lambda_{1,1}, \lambda_{2,1}, \lambda_{3,1}, \omega_1) = (3 + \omega_1 - \omega_1\lambda_{3,1})(\boldsymbol{P}_{3,1} - \boldsymbol{P}_{2,1}) \\ \boldsymbol{L}'_2(0; \lambda_{1,2}, \lambda_{2,2}, \lambda_{3,2}, \omega_2) = (3 + \omega_2 - \omega_2\lambda_{1,2})(\boldsymbol{P}_{1,2} - \boldsymbol{P}_{0,2}) \end{cases} \tag{7}$$

Finally, substituting (7) in (6) and combining with (5), we have

$$\boldsymbol{P}_{1,2} = \left[1 + \frac{3 + \omega_1 - \omega_1\lambda_{3,1}}{\alpha(3 + \omega_2 - \omega_2\lambda_{1,2})}\right] \boldsymbol{P}_{3,1} - \frac{3 + \omega_1 - \omega_1\lambda_{3,1}}{\alpha(3 + \omega_2 - \omega_2\lambda_{1,2})} \boldsymbol{P}_{2,1} \tag{8}$$

where $\alpha > 0$ is constant.

Consequently, (5) and (8) constitute the sufficient and necessary conditions for G^1 smooth continuity between two adjacent SG-Bézier curves. Obviously, when the constant $\alpha = 1$ in (2), the G^1 smooth continuity conditions in Theorem 1 will degrade into the sufficient and necessary conditions for C^1 smooth continuity between the curves. The greatest advantage of the smooth continuity between the SG-Bézier curves is that we can modify the shape of a composite curve just by changing its shape parameters (without modifying its control points) under the condition that the composite curve maintains G^1 or C^1 continuity condition.

3. Transfinite Vectored Rational Interpolating Function

As the basis of matrix-valued rational interpolating, vectored rational interpolating (VRI) is an extension of scalar functions rational interpolating, which has been widely applied in the field of graphics and image processing, data analysis, automatic control and mechanical vibration, and has aroused the interests of national and foreign scholars for researching and studying [20,21]. The definition of transfinite vectored rational interpolating (TVRI) function is given as follows on the basis of Samelson inverse.

Definition 1. Assuming $\boldsymbol{V} = (v_1, v_2, \ldots v_d)$ is a d-dimensional complex vector, namely, $\boldsymbol{V} \in \boldsymbol{C}^d$, the Samelson inverse of $\boldsymbol{V}$ is as follows [20,22]

$$\boldsymbol{V}^{-1} = \frac{1}{\boldsymbol{V}} = \boldsymbol{V}^* / \| \boldsymbol{V} \|^2 \tag{9}$$

where $\boldsymbol{V}^* = (v_1^*, v_2^*, \ldots v_d^*)$ is the conjugate vector of $\boldsymbol{V}$; $\| \boldsymbol{V} \|$ is the norm of $\boldsymbol{V}$ and $\| \boldsymbol{V} \|^2 = \boldsymbol{V} \cdot \boldsymbol{V}^* = (\boldsymbol{V}, \boldsymbol{V}^*)$.

The definition of TVRI function can be given according to the Samelson inverse of a vector in Definition 1. Since only three related interpolation conditions are involved in this paper, we just give the definition of bivariate TVRI function here.

Definition 2. First we can construct a bivariate function in the following form [20]

$$\boldsymbol{R}(s,t) = \frac{\boldsymbol{N}(s,t)}{q(s,t)} = \boldsymbol{b}_0(s) + \frac{t - t_0}{\boldsymbol{b}_1(s) + \frac{t-t_1}{\boldsymbol{b}_2(s)}} \tag{10}$$

If $\boldsymbol{R}(s,t)$ meets the following three interpolation conditions

$$\boldsymbol{R}(s,t_i) = \frac{\boldsymbol{N}(s,t_i)}{q(s,t_i)} = \boldsymbol{V}_i(s) \quad (i = 0,1,2) \tag{11}$$

Then $\boldsymbol{R}(s,t)$ is called the bivariate transfinite vectored rational interpolating function of the vectored functions $\boldsymbol{V}_i(s)(i = 0,1,2)$, or the BTVRI function for short. where $\boldsymbol{N}(s,t) = \{\lambda_1(s,t),\ \lambda_2(s,t), \lambda_3(s,t)\}$ is a three-dimensional vectored function, while $\lambda_j(s,t)$ $(j = 0,1,2)$ and $q(s,t)$ are real functions of the variable s and t; $\boldsymbol{V}_i(s), \boldsymbol{b}_i(s)(i = 0,1,2)$ are three-dimensional vectored functions of the variable $s, t_i \in \mathrm{R}^1(i = 0,1,2)$.

4. Construction of Shape-Adjustable Generalized Bézier Rotation Surfaces

4.1. Problem Description

In this section, the focus is mainly on how to construct SG-Bézier rotation surfaces in space by using the SG-Bézier curves. The construction for SG-Bézier rotation surfaces is that, given a composite SG-Bézier curve $\boldsymbol{L}_j(s; \lambda_{1,j}, \lambda_{2,j},$

$\lambda_{3,j}, \omega_j)$ $(0 \le s \le 1, j = 1, 2, \ldots, n)$, we can treat the curve as a generating line to construct a SG-Bézier rotation surface, and then to derive the explicit expression of the rotation surface based on the theory of BTVRI function. Due to the fact that a SG-Bézier rotation surface contains multiple independent shape parameters, we can modify the local or global shape of a rotation surface flexibly only by adjusting its shape parameters. Furthermore, by making use of the basic translational transformation and rotation transformation, the SG-Bézier rotation surfaces can be moved in any orientation to a specified location.

4.2. Construction Algorithm of SG-Bézier Rotation Surfaces

(1) In space rectangular coordinates system, we first construct a composite SG-Bézier curve $\tilde{\boldsymbol{L}}_0$ with shape adjustability in a plane $\sum$ (in order to simplify our discussion, $\sum$ can be considered as the plane xoy, the other two planes xoz and yoz can be discussed similarly). The curve is composed of n curved sections, whose control points are $\boldsymbol{P}_{0,j}, \boldsymbol{P}_{1,j}, \boldsymbol{P}_{2,j}, \boldsymbol{P}_{3,j} (j = 1, 2, \ldots, n)$.

According to (1), the expression of the curve $\tilde{\boldsymbol{L}}_0$ is

$$\boldsymbol{L}_{0,j}(s; \lambda_{1,j}, \lambda_{2,j}, \lambda_{3,j}, \omega_j) = \sum_{i=0}^{3} l_{i,4}(s) \boldsymbol{P}_{i,j}, \ (0 \le s \le 1, j = 1, 2, \ldots, n) \quad (12)$$

where $\boldsymbol{L}_{0,j}(s; \lambda_{1,j}, \lambda_{2,j}, \lambda_{3,j}, \omega_j)$ is the j-th curved section of $\tilde{\boldsymbol{L}}_0$, and $\lambda_{1,j}, \lambda_{2,j}$, $\lambda_{3,j}, \omega_j$ are its shape parameters; Each pair of neighboring curved sections $\boldsymbol{L}_{0,j}(s)$ and $\boldsymbol{L}_{0,j+1}(s)$ of $\tilde{\boldsymbol{L}}_0$ satisfies the G^0, G^1 or C^1 smooth continuity, in other words, meets the conditions for the G^0, G^1 or C^1 smooth continuity. The calculation formulas of the basis functions $l_{i,4}(s) (i = 0, 1, 2, 3)$ are as follows:

$$\begin{cases} l_{0,4}(s) = [1 + (\lambda_{1,j} - 1)\omega_j s](1 - s)^3 \\ l_{1,4}(s) = [3 + \omega_j(1 - \lambda_{1,j}) + \omega_j(\lambda_{1,j} + \lambda_{2,j} - 4)s]s(1 - s)^2 \\ l_{2,4}(s) = [3 + (3 - \lambda_{2,j})\omega_j - \omega_j(\lambda_{3,j} - \lambda_{2,j} + 2)s]s^2(1 - s) \\ l_{3,4}(s) = [1 + (\lambda_{3,j} - 1)\omega_j(1 - s)]s^3 \end{cases} \quad (13)$$

Let $\{x_{i,j}, y_{i,j}, 0\} (i = 0, 1, 2, 3; j = 1, 2, \ldots, n)$ be the coordinates of the control points $\boldsymbol{P}_{i,j} (i = 0, 1, 2, 3; j = 1, 2, \ldots, n)$. We can rewrite the expression of $\tilde{\boldsymbol{L}}_0$ in vector form as follows

$$\begin{aligned} \boldsymbol{L}_{0,j}(s; \lambda_{1,j}, \lambda_{2,j}, \lambda_{3,j}, \omega_j) &= \sum_{i=0}^{3} l_{i,4}(s) \boldsymbol{P}_{i,j} = \sum_{i=0}^{3} l_{i,4}(s) \{x_{i,j}, y_{i,j}, 0\} \\ &= \left\{ \sum_{i=0}^{3} l_{i,4}(s) x_{i,j}, \sum_{i=0}^{3} l_{i,4}(s) y_{i,j}, 0 \right\} \\ &= \{x_{0,j}(s), \ y_{0,j}(s), \ 0\} \ \ (0 \le s \le 1, j = 1, 2, \ldots, n) \end{aligned} \quad (14)$$

where $x_{0,j}(s) = \sum_{i=0}^{3} l_{i,4}(s) x_{i,j}, y_{0,j}(s) = \sum_{i=0}^{3} l_{i,4}(s) y_{i,j} (j = 1, 2, \ldots, n)$.

Next, construct a curve $\tilde{\mathbf{L}}_1$ in the plane xoz(noting: the plane is perpendicular to the plane xoy; the x-axis is the rotation axis of the rotation surface), and the curve can be expressed in the following vector function form

$$\begin{aligned} &\boldsymbol{L}_{1,j}(s;\lambda_{1,j},\lambda_{2,j},\lambda_{3,j},\omega_j) = \{x_{1,j}(s),\ 0,\ z_{1,j}(s)\} \\ &\quad = \{x_{0,j}(s),\ 0,\ y_{0,j}(s)\}(0 \le s \le 1, j = 1,2,\ldots,n) \end{aligned} \tag{15}$$

where $\boldsymbol{L}_{1,j}(s;\lambda_{1,j},\lambda_{2,j},\lambda_{3,j},\omega_j)$ is the j-th section of the composite curve $\tilde{\boldsymbol{L}}_1$, and it can be obtained by rotating the j-th section of the composite curve $\tilde{\boldsymbol{L}}_0$, namely $\boldsymbol{L}_{0,j}(s;\lambda_{1,j},\lambda_{2,j},\lambda_{3,j},\omega_j)$, clockwise around the x-axis with 90°.

Finally, let the x-axis be the symmetry axis L and calculate the composite curve $\tilde{\boldsymbol{L}}_2$ which is symmetric to the $\tilde{\boldsymbol{L}}_0$ about L, then we have

$$\begin{aligned} &\boldsymbol{L}_{2,j}(s;\lambda_{1,j},\lambda_{2,j},\lambda_{3,j},\omega_j) = \{x_{2,j}(s),\ y_{2,j}(s),\ 0\} \\ &\quad = \{x_{0,j}(s),\ -y_{0,j}(s),\ 0\}(0 \le s \le 1, j = 1,2,\ldots,n) \end{aligned} \tag{16}$$

where $\boldsymbol{L}_{2,j}(s;\lambda_{1,j},\lambda_{2,j},\lambda_{3,j},\omega_j)$ is the j-th curved section of the composite curve $\tilde{\boldsymbol{L}}_2$ and it is symmetric to $\boldsymbol{L}_{0,j}(s)$ about the x-axis.

Synthesizing the above results, we obtain the following three space parametric curves located in the plane xoy and xoz(the two planes are perpendicular to each other) respectively:

$$\begin{cases} \tilde{\boldsymbol{L}}_0 : \ \boldsymbol{L}_{0,j}(s;\lambda_{1,j},\lambda_{2,j},\lambda_{3,j},\omega_j) = \{x_{0,j}(s),\ y_{0,j}(s),\ 0\} \\ \tilde{\boldsymbol{L}}_1 : \ \boldsymbol{L}_{1,j}(s;\lambda_{1,j},\lambda_{2,j},\lambda_{3,j},\omega_j) = \{x_{0,j}(s),\ 0,\ y_{0,j}(s)\} \\ \tilde{\boldsymbol{L}}_2 : \ \boldsymbol{L}_{2,j}(s;\lambda_{1,j},\lambda_{2,j},\lambda_{3,j},\omega_j) = \{x_{0,j}(s),\ -y_{0,j}(s),\ 0\} \end{cases} \tag{17}$$

where $\lambda_{1,j},\lambda_{3,j} \in [0,4], \lambda_{2,j} \in [0,6],\ \omega_j \in [0,1]$, and $0 \le s \le 1, j = 1,2,\ldots,n$.

(2) Use the three curves $\boldsymbol{L}_{0,j}(s), \boldsymbol{L}_{1,j}(s)$ and $\boldsymbol{L}_{2,j}(s)$ in (17) as the three interpolation condition functions of the BTVRI function in (11), and then a BTVRI function similar to (10) can be constructed. The concrete steps are as follows:

Step 1 Let $t_0 = 0, t_1 = 1/2$ and $t_2 = 1$. According to the definition of (10), a three-dimensional vectored function can be defined as follows

$$\boldsymbol{b}_{0,j}(s;\lambda_{1,j},\lambda_{2,j},\lambda_{3,j},\omega_j) = \boldsymbol{L}_{0,j}(s;\lambda_{1,j},\lambda_{2,j},\lambda_{3,j},\omega_j)\ (j = 1,2,\ldots,n) \tag{18}$$

Step 2 On the basis of the definition of Samelson inverse, suppose $\boldsymbol{R}_{1,j}(s,t_1;\lambda_{1,j},\lambda_{2,j},\lambda_{3,j},\omega_j)$ satisfies

$$\begin{aligned} &\boldsymbol{R}_{1,j}(s,t_1;\lambda_{1,j},\lambda_{2,j},\lambda_{3,j},\omega_j) \\ &\quad = \frac{t_1 - t_0}{\boldsymbol{L}_{1,j}(s;\lambda_{1,j},\lambda_{2,j},\lambda_{3,j},\omega_j) - \boldsymbol{b}_{0,j}(s;\lambda_{1,j},\lambda_{2,j},\lambda_{3,j},\omega_j)} \end{aligned}$$

Then combined with (18), $\boldsymbol{R}_{1,j}(s,t_1;\lambda_{1,j},\lambda_{2,j},\lambda_{3,j},\omega_j)$ can be rewritten as follows

$$\begin{aligned}\boldsymbol{b}_{1,j}(s;\lambda_{1,j},\lambda_{2,j},\lambda_{3,j},\omega_j) &= \boldsymbol{R}_{1,j}(s,t_1;\lambda_{1,j},\lambda_{2,j},\lambda_{3,j},\omega_j)\\ &= \frac{t_1-t_0}{\boldsymbol{L}_{1,j}(s;\lambda_{1,j},\lambda_{2,j},\lambda_{3,j},\omega_j)-\boldsymbol{L}_{0,j}(s;\lambda_{1,j},\lambda_{2,j},\lambda_{3,j},\omega_j)}\ (j=1,2,\ldots,n)\end{aligned} \tag{19}$$

Step 3 Give the following definitions in turn

$$\begin{aligned}&\boldsymbol{R}_{1,j}(s,t_2;\lambda_{1,j},\lambda_{2,j},\lambda_{3,j},\omega_j)\\ &\quad= \frac{t_2-t_0}{\boldsymbol{L}_{2,j}(s;\lambda_{1,j},\lambda_{2,j},\lambda_{3,j},\omega_j)-\boldsymbol{b}_{0,j}(s;\lambda_{1,j},\lambda_{2,j},\lambda_{3,j},\omega_j)}\\ &\quad= \frac{t_2-t_0}{\boldsymbol{L}_{2,j}(s;\lambda_{1,j},\lambda_{2,j},\lambda_{3,j},\omega_j)-\boldsymbol{L}_{0,j}(s;\lambda_{1,j},\lambda_{2,j},\lambda_{3,j},\omega_j)}\\ &\boldsymbol{R}_{2,j}(s,t_2;\lambda_{1,j},\lambda_{2,j},\lambda_{3,j},\omega_j)\\ &\quad= \frac{t_2-t_1}{\boldsymbol{R}_{1,j}(s,t_2;\lambda_{1,j},\lambda_{2,j},\lambda_{3,j},\omega_j)-\boldsymbol{b}_{1,j}(s;\lambda_{1,j},\lambda_{2,j},\lambda_{3,j},\omega_j)}\end{aligned}$$

Therefore $\boldsymbol{R}_{2,j}(s,t_2;\lambda_{1,j},\lambda_{2,j},\lambda_{3,j},\omega_j)$ can be rewritten as

$$\begin{aligned}\boldsymbol{b}_{2,j}(s;\lambda_{1,j},\lambda_{2,j},\lambda_{3,j},\omega_j) &= \boldsymbol{R}_{2,j}(s,t_1;\lambda_{1,j},\lambda_{2,j},\lambda_{3,j},\omega_j)\\ &= (t_2-t_1)\left[\frac{t_2-t_0}{\boldsymbol{L}_{2,j}(s;\lambda_{1,j},\lambda_{2,j},\lambda_{3,j},\omega_j)-\boldsymbol{L}_{0,j}(s;\lambda_{1,j},\lambda_{2,j},\lambda_{3,j},\omega_j)}\right.\\ &\quad\left.-\frac{t_1-t_0}{\boldsymbol{L}_{1,j}(s;\lambda_{1,j},\lambda_{2,j},\lambda_{3,j},\omega_j)-\boldsymbol{L}_{0,j}(s;\lambda_{1,j},\lambda_{2,j},\lambda_{3,j},\omega_j)}\right]^{-1}\end{aligned} \tag{20}$$

where $\boldsymbol{L}_{i,j}(s;\lambda_{1,j},\lambda_{2,j},\lambda_{3,j},\omega_j)(i=0,1,2;\ j=1,2,\ldots,n)$ are defined in (17).

Step 4 Substitute $\boldsymbol{b}_{i,j}(s;\lambda_{1,j},\lambda_{2,j},\lambda_{3,j},\omega_j)(i=0,1,2;\ j=1,2,\ldots,n)$ obtained by (18)–(20) in (10), and then we can obtain the following BTVRI function

$$\begin{cases}\boldsymbol{R}_j(s,t;\lambda_{1,j},\lambda_{2,j},\lambda_{3,j},\omega_j)\\ \quad=\boldsymbol{b}_{0,j}(s;\lambda_{1,j},\lambda_{2,j},\lambda_{3,j},\omega_j)+\frac{t-t_0}{\boldsymbol{b}_{1,j}(s;\lambda_{1,j},\lambda_{2,j},\lambda_{3,j},\omega_j)+\frac{t-t_1}{\boldsymbol{b}_{2,j}(s;\lambda_{1,j},\lambda_{2,j},\lambda_{3,j},\omega_j)}}\\ 0\le s,t\le 1;\ 0\le\lambda_{1,j},\lambda_{3,j}\le 4, 0\le\lambda_{2,j}\le 6,\ 0\le\omega_j\le 1\\ \quad j=1,2,\ldots,n\end{cases} \tag{21}$$

It can be easily proved that the BTVRI function in (21) satisfies the following interpolation condition

$$\begin{aligned}&\boldsymbol{R}_j(s,t_i;\lambda_{1,j},\lambda_{2,j},\lambda_{3,j},\omega_j)\\ &\quad=\boldsymbol{L}_{i,j}(s,t_i;\lambda_{1,j},\lambda_{2,j},\lambda_{3,j},\omega_j)(i=0,1,2;\ j=1,2,\ldots,n)\end{aligned}$$

(3) Substitute the coordinates of the three space parametric curves of (17) in (21), and rationalize the functions $\boldsymbol{R}_j(s,t)$ in (21) from back to front by using the Samelson inverse, which means

$$
\begin{aligned}
&\boldsymbol{R}_j(s,t;\lambda_{1,j},\lambda_{2,j},\lambda_{3,j},\omega_j)\\
&\quad=\boldsymbol{b}_{0,j}(s;\lambda_{1,j},\lambda_{2,j},\lambda_{3,j},\omega_j)\\
&\qquad+\frac{t-t_0}{\boldsymbol{b}_{1,j}(s;\lambda_{1,j},\lambda_{2,j},\lambda_{3,j},\omega_j)+\frac{t-t_1}{\boldsymbol{b}_{2,j}(s;\lambda_{1,j},\lambda_{2,j},\lambda_{3,j},\omega_j)}}\\
&\quad=\{x_{0,j}(s),\ y_{0,j}(s),\ 0\}+\frac{t-0}{\frac{0.5}{\{0,\ -y_{0,j}(s),\ y_{0,j}(s)\}}+\frac{t-0.5}{\{0,\ -y_{0,j}(s),\ -y_{0,j}(s)\}}}\\
&\quad=\{x_{0,j}(s),\ y_{0,j}(s),\ 0\}+\frac{t-0}{\frac{\{0,\ -y_{0,j}(s),\ y_{0,j}(s)\}}{4y_{0,j}^2(s)}+\frac{(t-0.5)\{0,\ -y_{0,j}(s),\ -y_{0,j}(s)\}}{2y_{0,j}^2(s)}}\\
&\quad=\{x_{0,j}(s),\ y_{0,j}(s),\ 0\}+\frac{t}{\left\{0,\ -\frac{t}{2y_{0,j}(s)},\ \frac{1-t}{2y_{0,j}(s)}\right\}}\\
&\quad=\{x_{0,j}(s),\ y_{0,j}(s),\ 0\}+\frac{t}{2t^2-2t+1}\{0,\ -2ty_{0,j}(s),\ 2(1-t)y_{0,j}(s)\}\\
&\quad=\left\{x_{0,j}(s),\ \frac{1-2t}{2t^2-2t+1}y_{0,j}(s),\ \frac{2t-2t^2}{2t^2-2t+1}y_{0,j}(s)\right\}
\end{aligned}
\tag{22}
$$

Consequently, (22) gives the explicit expression of the BTVRI functions $\boldsymbol{R}_j(s,t;\lambda_{1,j},\lambda_{2,j},\lambda_{3,j},\omega_j)$. In order to facilitate our following discussion, $\boldsymbol{R}_j(s,t)$ can be rewritten in the following form with new introduced symbols

$$
\begin{aligned}
\boldsymbol{R}_j(s,t;\lambda_{1,j},\lambda_{2,j},\lambda_{3,j},\omega_j)&=\frac{\boldsymbol{N}_j(s,t)}{q_j(s,t)}\\
&=\{r_{1,j}(s,t;\lambda_{1,j},\lambda_{2,j},\lambda_{3,j},\omega_j),\ r_{2,j}(s,t;\lambda_{1,j},\lambda_{2,j},\lambda_{3,j},\omega_j),\\
&\quad r_{3,j}(s,t;\lambda_{1,j},\lambda_{2,j},\lambda_{3,j},\omega_j)\}
\end{aligned}
\tag{23}
$$

where the calculating formulas for $r_{i,j}(s,t)(i=1,2,3)$are

$$
\begin{cases}
r_{1,j}(s,t;\lambda_{1,j},\lambda_{2,j},\lambda_{3,j},\omega_j)=x_{0,j}(s)\\
r_{2,j}(s,t;\lambda_{1,j},\lambda_{2,j},\lambda_{3,j},\omega_j)=\frac{1-2t}{2t^2-2t+1}y_{0,j}(s)\\
r_{3,j}(s,t;\lambda_{1,j},\lambda_{2,j},\lambda_{3,j},\omega_j)=\frac{2t-2t^2}{2t^2-2t+1}y_{0,j}(s)\\
\quad j=1,2,\ldots,n
\end{cases}
\tag{24}
$$

here $x_{0,j}(s),y_{0,j}(s)(j=1,2,\ldots,n)$ can be calculated according to (14).

On the basis of the conclusions in [20,23], it is easy to prove that the parametric surface represented by (23) is half of the rotation surface generated by rotating the generating line $\tilde{\boldsymbol{L}}_0$ in the plane xoy with a revolution around the x-axis (the process of proof is not covered again here).

(4) If the whole rotation surface is required, the other half of it can be obtained by using the opposite sign of the component $r_{3,j}(s,t;\lambda_{1,j},\lambda_{2,j},\lambda_{3,j},\omega_j)$ of $\boldsymbol{R}_j(s,t;\lambda_{1,j},\lambda_{2,j},\lambda_{3,j},\omega_j)$, that is

$$
\begin{aligned}
&\tilde{\boldsymbol{R}}_j(s,t;\lambda_{1,j},\lambda_{2,j},\lambda_{3,j},\omega_j)\\
&\quad=\{r_{1,j}(s,t;\lambda_{1,j},\lambda_{2,j},\lambda_{3,j},\omega_j),\ r_{2,j}(s,t;\lambda_{1,j},\lambda_{2,j},\lambda_{3,j},\omega_j),\\
&\qquad -r_{3,j}(s,t;\lambda_{1,j},\lambda_{2,j},\lambda_{3,j},\omega_j)\}
\end{aligned}
$$

Hence, the equation of the whole rotation surface generated by rotating the generating line $\tilde{\boldsymbol{L}}_0$ with one revolution around the x-axis is

$$\begin{cases} \boldsymbol{R}_j(s,t;\lambda_{1,j},\lambda_{2,j},\lambda_{3,j},\omega_j) \\ \quad = \{r_{1,j}(s,t;\lambda_{1,j},\lambda_{2,j},\lambda_{3,j},\omega_j),\ r_{2,j}(s,t;\lambda_{1,j},\lambda_{2,j},\lambda_{3,j},\omega_j), \\ r_{3,j}(s,t;\lambda_{1,j},\lambda_{2,j},\lambda_{3,j},\omega_j)\} \\ \tilde{\boldsymbol{R}}_j(s,t;\lambda_{1,j},\lambda_{2,j},\lambda_{3,j},\omega_j) \\ \quad = \{r_{1,j}(s,t;\lambda_{1,j},\lambda_{2,j},\lambda_{3,j},\omega_j),\ r_{2,j}(s,t;\lambda_{1,j},\lambda_{2,j},\lambda_{3,j},\omega_j)\ , \\ \qquad -r_{3,j}(s,t;\lambda_{1,j},\lambda_{2,j},\lambda_{3,j},\omega_j)\} \\ \quad 0\le s,t\le 1;\ 0\le \lambda_{1,j},\lambda_{3,j}\le 4, 0\le \lambda_{2,j}\le 6,\ 0\le \omega_j\le 1;\ j=1,2,\ldots,n \end{cases} \tag{25}$$

where $\boldsymbol{R}_j(s,t;\lambda_{1,j},\lambda_{2,j},\lambda_{3,j},\omega_j)$ and $\tilde{\boldsymbol{R}}_j(s,t;\lambda_{1,j},\lambda_{2,j},\lambda_{3,j},\omega_j)$ are symmetrical about the plane xoy and they make up a whole rotation surface; Their three components $r_{i,j}(s,t;\lambda_{1,j},\lambda_{2,j},\lambda_{3,j},\omega_j)(i=1,2,3)$ are calculated according to (24).

Furthermore, if we want to get a partial rotation surface generated by rotating the generating line $\tilde{\boldsymbol{L}}_0$ around the x-axis with a fixed angle $\theta(0<\theta<2\pi;\theta\neq\pi)$, the following ways can be taken to solve this problem: ①If the rotation angle satisfies $0<\theta<\pi$, we only need to use $\boldsymbol{R}_j(s,t;\lambda_{1,j},\lambda_{2,j},\lambda_{3,j},\omega_j)$ in (25) to generate the partial rotation surface and the value range of the parameter t becomes $0\le t\le\theta/\pi$ in this case; ② If the rotation angle satisfies $\pi<\theta<2\pi$, we can use $\boldsymbol{R}_j(s,t;\lambda_{1,j},\lambda_{2,j},\lambda_{3,j},\omega_j)$ to generate the first half and then use $\tilde{\boldsymbol{R}}_j(s,t;\lambda_{1,j},\lambda_{2,j},\lambda_{3,j},\omega_j)$ to generate the rest according to the method in ①, with the value range of the parameter t becoming $0\le t\le\theta/\pi$.

In conclusion, if the generating line locates in the plane xoz or yoz and the rotation axis is the z-axis or y-axis, we can also construct a rotation surface and reach similar conclusions.

Theorem 2. *In the plane xoz, given a set of control points* $\boldsymbol{P}_{i,j}(i=0,1,2,3;j=1,2,\ldots,n)$ *whose coordinates are taken as* $\{x_{i,j},0,z_{i,j}\}(i=0,1,2,3;j=1,2,\ldots,n)$, *then a composite SG-Bézier curve* $\tilde{\boldsymbol{L}}_0^Z$ *can be constructed by these control points. The equation of the whole rotation surface generated by rotating the generating line* $\tilde{\boldsymbol{L}}_0^Z$ *around the z-axis with one revolution is*

$$\begin{cases} \boldsymbol{R}_j^Z(s,t;\lambda_{1,j},\lambda_{2,j},\lambda_{3,j},\omega_j)=\left\{\frac{1-2t}{2t^2-2t+1}x_{0,j}(s),\ \ \frac{2t-2t^2}{2t^2-2t+1}x_{0,j}(s),\ z_{0,j}(s)\right\} \\ \tilde{\boldsymbol{R}}_j^Z(s,t;\lambda_{1,j},\lambda_{2,j},\lambda_{3,j},\omega_j)=\left\{\frac{1-2t}{2t^2-2t+1}x_{0,j}(s),\ \ -\frac{2t-2t^2}{2t^2-2t+1}x_{0,j}(s),\ z_{0,j}(s)\right\} \end{cases} \tag{26}$$

where $0\le s,t\le 1,\lambda_{1,j},\lambda_{3,j}\in[0,4],\lambda_{2,j}\in[0,6],\ \omega_j\in[0,1](j=1,2,\ldots,n)$ *are shape parameters;* $\boldsymbol{R}_j^Z$ *and* $\tilde{\boldsymbol{R}}_j^Z$ *are symmetrical about the plane xoz; combined with the two expressions, we can construct a whole SG-Bézier rotation surface. For the j-th curved section* $\boldsymbol{L}_{0,j}^Z$ *of the generating line* $\tilde{\boldsymbol{L}}_0^Z$, *the calculating formulas of its components* $x_{0,j}(s)$ *and* $z_{0,j}(s)$ *are*

$$\begin{cases} x_{0,j}(s) = \sum_{i=0}^{3} l_{i,4}(s) x_{i,j} \\ z_{0,j}(s) = \sum_{i=0}^{3} l_{i,4}(s) z_{i,j} \end{cases}$$

where the basis functions $l_{i,4}(s)(i = 0, 1, 2, 3)$ *are calculated according to* (13).

Theorem 3. *In the plane yoz, given a set of control points* $\boldsymbol{P}_{i,j}(i = 0, 1, 2, 3; j = 1, 2, \ldots, n)$ *whose coordinates are taken as* $\{0, y_{i,j}, z_{i,j}\}(i = 0, 1, 2, 3; j = 1, 2, \ldots, n)$, *then a composite SG-Bézier curve* $\tilde{\boldsymbol{L}}_0^Y$ *can be constructed by these control points. And the equation of the whole rotation surface generated by rotating the generating line* $\tilde{\boldsymbol{L}}_0^Y$ *around the y-axis with one revolution is*

$$\begin{cases} \boldsymbol{R}_j^Y(s,t;\lambda_{1,j},\lambda_{2,j},\lambda_{3,j},\omega_j) = \left\{ \frac{2t-2t^2}{2t^2-2t+1} z_{0,j}(s),\ \ y_{0,j}(s),\ \ \frac{1-2t}{2t^2-2t+1} z_{0,j}(s) \right\} \\ \tilde{\boldsymbol{R}}_j^Y(s,t;\lambda_{1,j},\lambda_{2,j},\lambda_{3,j},\omega_j) = \left\{ -\frac{2t-2t^2}{2t^2-2t+1} z_{0,j}(s),\ \ y_{0,j}(s),\ \ \frac{1-2t}{2t^2-2t+1} z_{0,j}(s) \right\} \end{cases} \tag{27}$$

where $0 \le s, t \le 1, \lambda_{1,j}, \lambda_{3,j} \in [0, 4], \lambda_{2,j} \in [0, 6],\ \omega_j \in [0, 1](j = 1, 2, \ldots, n)$ *are shape parameters;* $\boldsymbol{R}_j^Y$ *and* $\tilde{\boldsymbol{R}}_j^Y$ *are symmetrical about the plane yoz; combined with the two expressions in* (27), *we can construct a whole SG-Bézier rotation surface. For the j-th curved section* $\boldsymbol{L}_{0,j}^Y$ *of the generating line* $\tilde{\boldsymbol{L}}_0^Y$, *the calculating formulas of its components* $y_{0,j}(s)$ *and* $z_{0,j}(s)$ *are*

$$\begin{cases} y_{0,j}(s) = \sum_{i=0}^{3} l_{i,4}(s) y_{i,j} \\ z_{0,j}(s) = \sum_{i=0}^{3} l_{i,4}(s) z_{i,j} \end{cases}$$

where the basis functions $l_{i,4}(s)(i = 0, 1, 2, 3)$ *are calculated according to (13)*

4.3. Properties Analysis of SG-Bézier Rotation Surfaces

Due to the fact that the generating line of a SG-Bézier rotation surface is a SG-Bézier curve, the SG-Bézier rotation surfaces inherit many excellent properties of SG-Bézier curves.

(1) Properties of boundary interpolation. The terminal properties of the SG-Bézier curves tell us, for any piece of the generating line $\tilde{\boldsymbol{L}}_0$ of the SG-Bézier rotation surfaces in (25), $\boldsymbol{L}_{0,j}(s;\lambda_{1,j},\lambda_{2,j},\lambda_{3,j},\omega_j)(j = 1, 2, \ldots, n)$ interpolates through its terminal control points $\boldsymbol{P}_{0,j}$ and $\boldsymbol{P}_{3,j}$, and the control points for each pair of adjacent curves $\boldsymbol{L}_{0,j}(s)$ and $\boldsymbol{L}_{0,j+1}(s)$ satisfy $\boldsymbol{P}_{3,j} = \boldsymbol{P}_{0,j+1}(j = 1, 2, \ldots, n-1)$. Therefore, the SG-Bézier rotation surfaces in (25) interpolate through the $n+1$ circles generated by rotating its control points $\boldsymbol{P}_{0,j}, \boldsymbol{P}_{3,j}(j = 1, 2, \ldots, n)$ around the x-axis with one revolution.

(2) Convex hull properties. The SG-Bézier rotation surfaces in (25) locate within the stereoscopic rotation convex hull in space generated by rotating the convex hull of its generating line $\tilde{\boldsymbol{L}}_0$ around the x-axis with one revolution.

(3) Smoothness. If each pair of the adjacent curved sections $\boldsymbol{L}_{0,j}(s)$ and $\boldsymbol{L}_{0,j+1}(s)$ of the generating line $\tilde{\boldsymbol{L}}_0$ achieves G^0, G^1 or C^1 smooth continuity,

then the generated SG-Bézier rotation surface would surely achieves G^0, G^1 or C^1 smooth continuity along the direction of its generating line $\tilde{\boldsymbol{L}}_0$.

(4) Approximation property. With the gradual decrease of the shape parameters $\lambda_{1,j}, \lambda_{2,j}, \lambda_{3,j}$ and ω_j, the SG-Bézier curve approaches its control polygon little by little; Thus, the generated SG-Bézier rotation surface will also gradually approaches the rotation surface generated by rotating the control polygon of its generating line $\tilde{\boldsymbol{L}}_0$ around the x-axis with one revolution in this case.

4.4. Influence Rules of Shape Parameters on the SG-Bézier Rotation Surfaces

As shape parameters play a key role in the shape control of the SG-Bézier rotation surfaces, it is necessary to analyze the influence rules of the shape parameters. The SG-Bézier rotation surfaces contain the $4n$ independent shape parameters $\lambda_{1,j}, \lambda_{2,j}, \lambda_{3,j}, \omega_j (j = 1, 2, \ldots, n)$, and we can analyze the influence rules according to the influence rules of its shape parameters on its generating line. Further more, we can modify the shape of the SG-Bézier rotation surfaces in $\mathrm{C}_3^1 \cdot \mathrm{C}_3^1 \cdot \mathrm{C}_3^1 \cdot \mathrm{C}_3^1 - 1 = 80$ different ways by adjusting the values of $\lambda_{1,j}, \lambda_{2,j}, \lambda_{3,j}, \omega_j$, achieving the local and global shape modification of the rotation surface.

The influence rules of the shape parameters on the SG-Bézier rotation surfaces are as follows: ① With the gradual decrease or increase of the shape parameter $\lambda_{1,j}$(all other parameters maintaining unchanged and $\omega_j \neq 0$), the rotation surfaces $\boldsymbol{R}_j(s,t), \tilde{\boldsymbol{R}}_j(s,t)$ will gradually approach or move away from the circle generated by rotating the control point $\boldsymbol{P}_{1,j}$ of the rotation generating line $\tilde{\boldsymbol{L}}_0$ around x-axis with one revolution. ② With the gradual decrease or increase of the shape parameter $\lambda_{3,j}$ (all other parameters maintaining unchanged and $\omega_j \neq 0$), the rotation surfaces $\boldsymbol{R}_j(s,t), \tilde{\boldsymbol{R}}_j(s,t)$ will gradually move away from or approach the circle generated by rotating the control point $\boldsymbol{P}_{2,j}$ of the rotation generating line $\tilde{\boldsymbol{L}}_0$ around x-axis with one revolution. ③ With the gradual increase of the shape parameter $\lambda_{2,j}$ (all other parameters maintaining unchanged and $\omega_j \neq 0$), the rotation surfaces $\boldsymbol{R}_j(s,t), \tilde{\boldsymbol{R}}_j(s,t)$ will gradually approach the circle generated by rotating the control point $\boldsymbol{P}_{1,j}$ of the rotation generating line $\tilde{\boldsymbol{L}}_0$ around x-axis with one revolution and move away from the one generated by rotating the control point $\boldsymbol{P}_{2,j}$ of the rotation generating line $\tilde{\boldsymbol{L}}_0$ around x-axis with one revolution. ④ The influence rules of the shape parameter ω_j on the shape of the SG-Bézier rotation surfaces can be divided into the following situations: (i) When $\lambda_{1,j} > 1$ and $\lambda_{3,j} > 1$, with the gradual decrease or increase of ω_j(all other shape parameters maintaining unchanged), the rotation surfaces $\boldsymbol{R}_j(s,t), \tilde{\boldsymbol{R}}_j(s,t)$ will gradually approach or move away from the rotation surface generated by rotating the control polygon of the generating line $\tilde{\boldsymbol{L}}_0$ around x-axis with one revolution; (ii) When $\lambda_{1,j} < 1$ and $\lambda_{3,j} < 1$, the influence rule is just the opposite from that of (i); (iii)When $\lambda_{1,j} < 1$ and $\lambda_{3,j} > 1$, with the gradual increase of ω_j (all other parameters

maintaining unchanged), the rotation surfaces $\boldsymbol{R}_j(s,t), \tilde{\boldsymbol{R}}_j(s,t)$ will gradually approach the circle generated by rotating the control point $\boldsymbol{P}_{1,j}$ around x-axis with one revolution and move away from the one generated by rotating the control point $\boldsymbol{P}_{2,j}$ around x-axis with one revolution; (iv) When $\lambda_{1,j} > 1$ and $\lambda_{3,j} < 1$, the influence rule is just the opposite from the situation of (iii); (v) When $\lambda_{1,j} = \lambda_{3,j} = 1, \lambda_{2,j} > 3$, the influence rule is just the same as that of (iii), while when $\lambda_{1,j} = \lambda_{3,j} = 1, \lambda_{2,j} < 3$, the influence rule is just the opposite from that of (iii); (vi)When $\lambda_1 = \lambda_3 = 1, \lambda_2 = 3$, the SG-Bézier rotation surfaces will degrade into the traditional cubic Bézier rotation surfaces, and ω_j will lose its effect in shape adjustability.

5. Numerical Examples

5.1. The Rotation of a SG-Bézier Curve Around the x-axis

Here, we give a numerical example to show the rotation of a shape-adjustable generalized Bézier curve around the x-axis at first. Given a set of control points $\boldsymbol{P}_j (j = 0, 1, 2, 3)$ in the plane xoy, whose coordinates are as follows:

$$\begin{cases} \boldsymbol{P}_0 = (0.2,\ 0.2,\ 0) \\ \boldsymbol{P}_1 = (0,\ 0.9,\ 0) \\ \boldsymbol{P}_2 = (1,\ 0.9,\ 0) \\ \boldsymbol{P}_3 = (0.8,\ 0.2,\ 0) \end{cases} \tag{28}$$

According to (14) and (28), the parametric equation of the SG-Bézier curves $\boldsymbol{L}_0(s; \lambda_1, \lambda_2, \lambda_3, \omega)$ defined by these control points $\boldsymbol{P}_j (j = 0, 1, 2, 3)$ is

$$\boldsymbol{L}_0(s; \lambda_1, \lambda_2, \lambda_3, \omega) = \{x_0(s),\ y_0(s),\ 0\} \ \ (0 \le s \le 1) \tag{29}$$

where

$$\begin{cases} x_0(s) = \frac{1}{5} + \left(-\frac{3}{5} + \frac{1}{5}\lambda_1\omega - \frac{1}{5}\omega\right) s + \left(\frac{18}{5}\omega - \frac{3}{5}\lambda_1\omega + \frac{18}{5} - \lambda_2\omega\right) s^2 \\ + \left(-\frac{12}{5} + 2\lambda_2\omega + \frac{3}{5}\lambda_1\omega - \frac{1}{5}\lambda_3\omega - \frac{32}{5}\omega\right) s^3 + \left(3\omega - \lambda_2\omega - \frac{1}{5}\lambda_1\omega + \frac{1}{5}\lambda_3\omega\right) s^4 \\ y_0(s) = \frac{1}{5} + \left(\frac{21}{10} + \frac{7}{10}\omega - \frac{7}{10}\lambda_1\omega\right) s + \left(\frac{21}{10}\lambda_1\omega - \frac{21}{10} - \frac{21}{10}\omega\right) s^2 \\ + \left(-\frac{21}{10}\lambda_1\omega + \frac{14}{5}\omega - \frac{10}{7}\lambda_3\omega\right) s^3 + \left(-\frac{7}{5}\omega + \frac{7}{10}\lambda_1\omega + \frac{7}{10}\lambda_3\omega\right) s^4 \end{cases} \tag{30}$$

here $0 \le \lambda_1, \lambda_3 \le 4, 0 \le \lambda_2 \le 6,\ 0 \le \omega \le 1$.

In terms of (25), the rotation surface generated by rotating the generating line $\boldsymbol{L}_0(s; \lambda_1, \lambda_2, \lambda_3, \omega)$ around the x-axis with one revolution is

$$\begin{cases} \boldsymbol{R}(s,t; \lambda_1, \lambda_2, \lambda_3, \omega) \\ \quad = \left\{x_0(s),\ \frac{1-2t}{2t^2-2t+1} y_0(s),\ \frac{2t-2t^2}{2t^2-2t+1} y_0(s)\right\} \\ \tilde{\boldsymbol{R}}(s,t; \lambda_1, \lambda_2, \lambda_3, \omega) \\ \quad = \left\{x_0(s),\ \frac{1-2t}{2t^2-2t+1} y_0(s),\ -\frac{2t-2t^2}{2t^2-2t+1} y_0(s)\right\} \\ \quad 0 \le s, t \le 1 \end{cases} \tag{31}$$

where $\boldsymbol{R}(s,t;\lambda_1,\lambda_2,\lambda_3,\omega)$ and $\tilde{\boldsymbol{R}}(s,t;\lambda_1,\lambda_2,\lambda_3,\omega)$ constitute a whole rotation surface and they are symmetrical about the plane xoy; $x_0(s)$ and $y_0(s)$ can be calculated according to the formulas in (30).

Figures 2, 3, 4 and 5 show some graphics of the SG-Bézier rotation surfaces with different shape parameters, where their generating lines have the same control polygon. In these figures, the green light mesh surfaces are the generating rotation surfaces, the yellow curves are the generating line $\boldsymbol{L}_0(s;\lambda_1,\lambda_2,\lambda_3,\omega)$, the blue polylines are the control polygon; The space circles composed of "*" are generated by rotating the control point $\boldsymbol{P}_1$ of the generating line $\boldsymbol{L}_0$ around the x-axis with one revolution, and the space circles composed of "o" are generated by rotating the control point $\boldsymbol{P}_2$ of the generating line $\boldsymbol{L}_0$ around the x-axis with one revolution. It can be seen from Figs. 2, 3, 4 and 5, with the varying of the shape parameters, the change rule of the shape of the rotation surface is consistent with the conclusion in Sect. 4.4. All of these mean that the shape of a SG-Bézier rotation surface can be modified handily by adjusting its four shape parameters, which reduces time and effort greatly.

Furthermore, using the method in this paper, we can also obtain the rotation surface generated by rotating the generating line $\boldsymbol{L}_0(s;\lambda_1,\lambda_2,\lambda_3,\omega)$ around the x-axis with a certain angle $\theta(0<\theta<2\pi;\theta\neq\pi)$, and the concrete processing method can be seen in the discussion in Sect. 4.2. Figure 6 shows some graphics of these incomplete SG-Bézier rotation surfaces generated by rotating the generating line $\boldsymbol{L}_0(s;\lambda_1,\lambda_2,\lambda_3,\omega)$ around the x-axis with the angle $\theta=0.5\pi$ and $\theta=1.4\pi$, and the shape parameters as well as control points of the generating line $\boldsymbol{L}_0(s;\lambda_1,\lambda_2,\lambda_3,\omega)$ are selected following the relative values in Fig. 2a.

5.2. The Rotation of Three Pieces of SG-Bézier Curves Around the z-axis

In this section, we give a numerical example to show the rotation of a generating line, which is constructed by joining three SG-Bézier curves together with piecewise smooth features (such as the G^1 or G^1 continuity), around the z-axis. Given a set of control points $\boldsymbol{P}_{i,j}(i=0,1,2,3;\ j=1,2,3)$ in the plane xoz, whose coordinates are as follows

$$\begin{cases} \boldsymbol{P}_{0,1}=(5,\ 0,\ 13), \boldsymbol{P}_{1,1}=(6,\ 0,\ 12) \\ \boldsymbol{P}_{2,1}=(3,\ 0,\ 10), \boldsymbol{P}_{3,1}=(2,\ 0,\ 8) \\ \boldsymbol{P}_{0,2}=\boldsymbol{P}_{3,1} \\ \boldsymbol{P}_{1,2}=(1,\ 0,\ 6) \\ \boldsymbol{P}_{2,2}=(2,\ 0,\ 3), \boldsymbol{P}_{3,2}=(5,\ 0,\ \text{-}1) \\ \boldsymbol{P}_{0,3}=\boldsymbol{P}_{3,2}, \\ \boldsymbol{P}_{1,3}=(8,\ 0,\ \text{-}5) \\ \boldsymbol{P}_{2,3}=(5,\ 0,\ \text{-}9), \boldsymbol{P}_{3,3}=(8,\ 0,\ \text{-}10) \end{cases} \tag{32}$$

According to (14) and (28), the parametric equations for the three pieces of SG-Bézier curves $\boldsymbol{L}^Z_{0,j}(s;\lambda_{1,j},\lambda_{2,j},\lambda_{3,j},\omega_j)$ defined by these control points

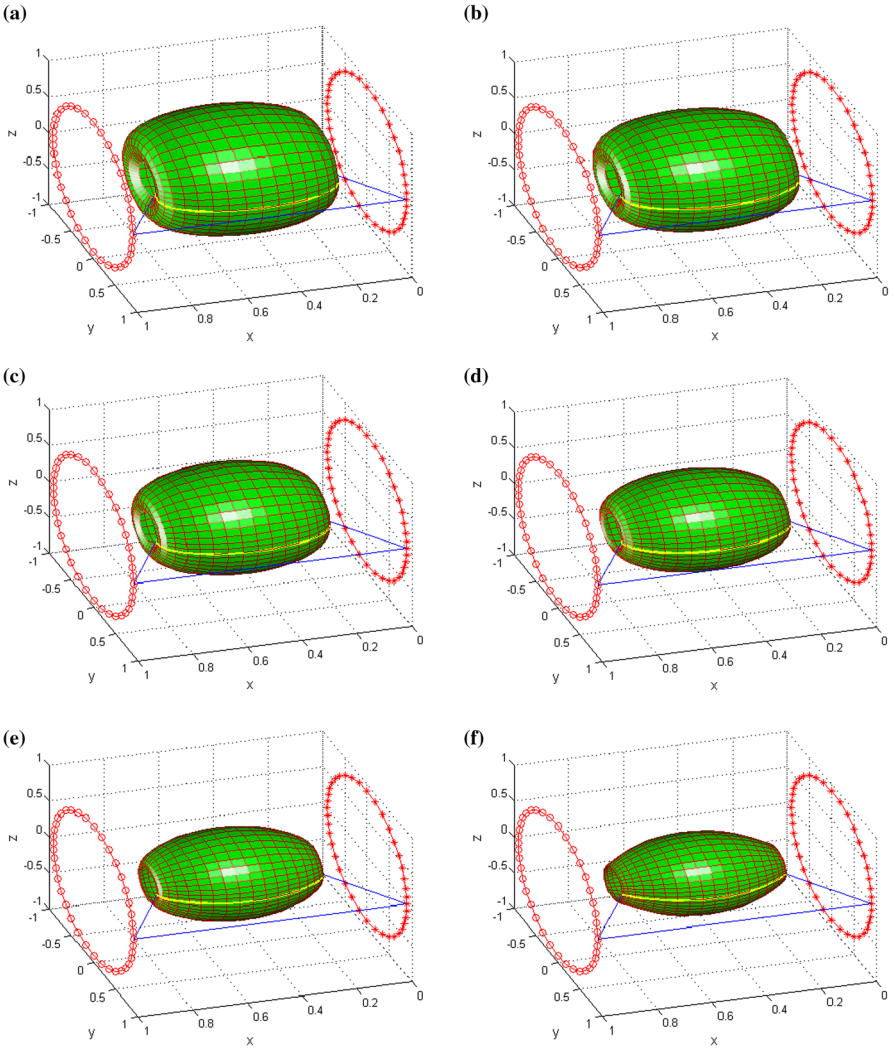

FIGURE 2. SG-Bézier rotation surfaces with the parameter ω taking different values and $\lambda_1, \lambda_2, \lambda_3$ keeping unchanged. **a** $\lambda_1 = 4, \lambda_2 = 3, \lambda_3 = 4; \omega = 0$. **b** $\lambda_1 = 4, \lambda_2 = 3, \lambda_3 = 4; \omega = 0.2$. **c** $\lambda_1 = 4, \lambda_2 = 3, \lambda_3 = 4; \omega = 0.4$. **d** $\lambda_1 = 4, \lambda_2 = 3, \lambda_3 = 4; \omega = 0.6$. **e** $\lambda_1 = 4, \lambda_2 = 3, \lambda_3 = 4; \omega = 0.8$ (**f**) $\lambda_1 = 4, \lambda_2 = 3, \lambda_3 = 4; \omega = 1$

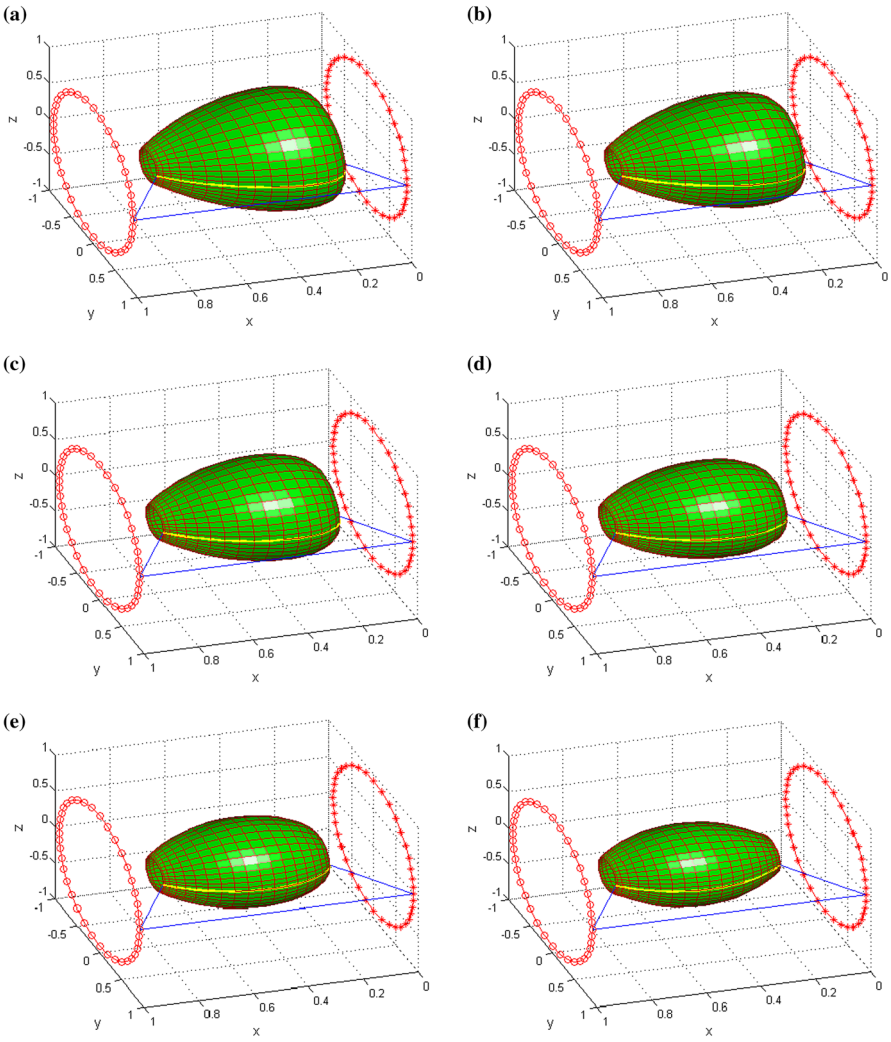

FIGURE 3. SG-Bézier rotation surfaces with the parameter λ_1 taking different values and $\omega, \lambda_2, \lambda_3$ keeping unchanged. **a** $\omega = 1, \lambda_2 = 3, \lambda_3 = 4; \lambda_1 = 0$. **b** $\omega = 1, \lambda_2 = 3, \lambda_3 = 4; \lambda_1 = 0.8$. **c** $\omega = 1, \lambda_2 = 3, \lambda_3 = 4; \lambda_1 = 1.6$. **d** $\omega = 1, \lambda_2 = 3, \lambda_3 = 4; \lambda_1 = 2.4$. **e** $\omega = 1, \lambda_2 = 3, \lambda_3 = 4; \lambda_1 = 3.2$. **f** $\omega = 1, \lambda_2 = 3, \lambda_3 = 4; \lambda_1 = 4$

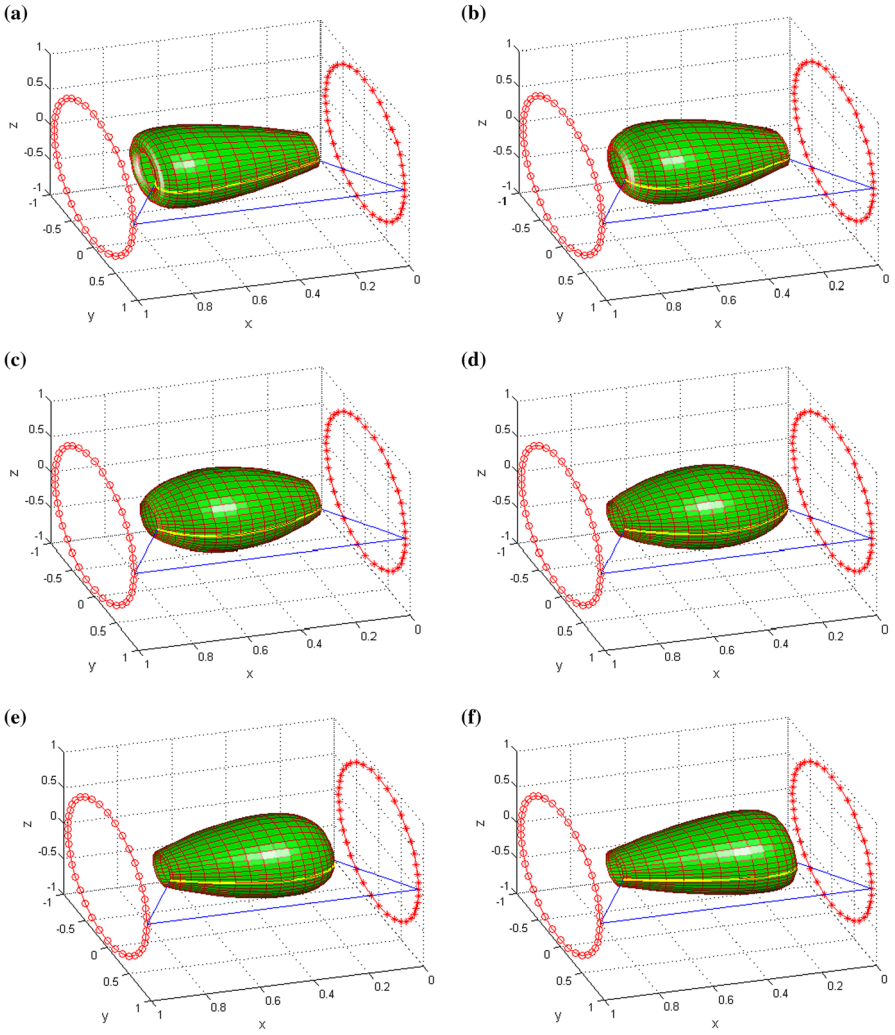

FIGURE 4. SG-Bézier rotation surfaces with the parameter λ_2 taking different values and $\lambda_1, \omega, \lambda_3$ keeping unchanged. **a** $\lambda_1 = 4, \omega = 1, \lambda_3 = 4; \lambda_2 = 0$. **b** $\lambda_1 = 4, \omega = 1, \lambda_3 = 4; \lambda_2 = 1.2$. **c** $\lambda_1 = 4, \omega = 1, \lambda_3 = 4; \lambda_2 = 2.4$. **d** $\lambda_1 = 4, \omega = 1, \lambda_3 = 4; \lambda_2 = 3.6$. **e** $\lambda_1 = 4, \omega = 1, \lambda_3 = 4; \lambda_2 = 4.8$. **f** $\lambda_1 = 4, \omega = 1, \lambda_3 = 4; \lambda_2 = 6$

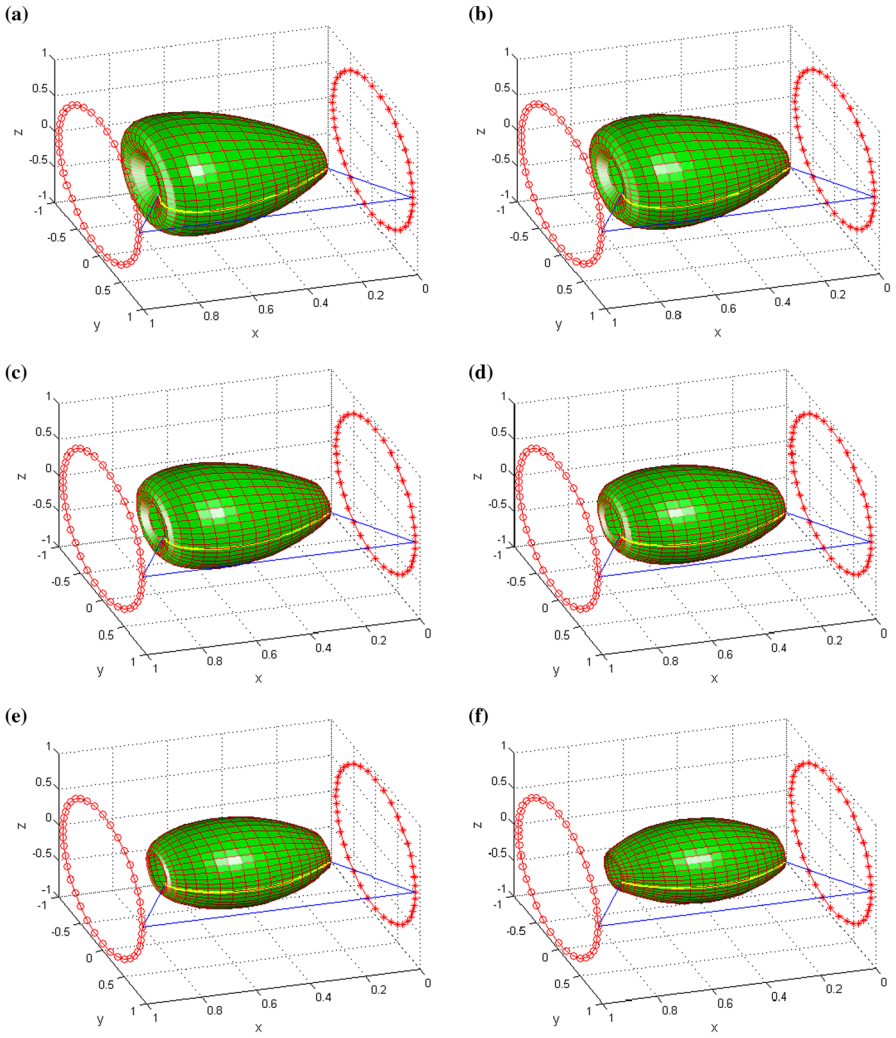

FIGURE 5. SG-Bézier rotation surfaces with the parameter λ_3 taking different values and $\lambda_1, \lambda_2, \omega$ keeping unchanged. **a** $\lambda_1 = 4, \lambda_2 = 3, \omega = 1; \lambda_3 = 0$. **b** $\lambda_1 = 4, \lambda_2 = 3, \omega = 1; \lambda_3 = 0.8$. **c** $\lambda_1 = 4, \lambda_2 = 3, \omega = 1; \lambda_3 = 1.6$. **d** $\lambda_1 = 4, \lambda_2 = 3, \omega = 1; \lambda_3 = 2.4$. **e** $\lambda_1 = 4, \lambda_2 = 3, \omega = 1; \lambda_3 = 3.2$. **f** $\lambda_1 = 4, \lambda_2 = 3, \omega = 1; \lambda_3 = 4$

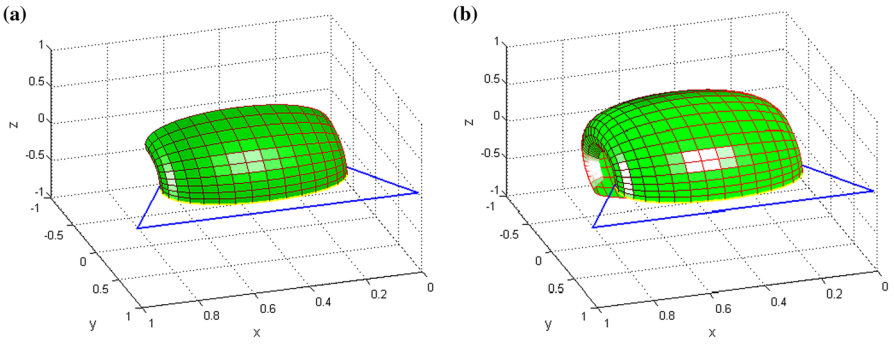

FIGURE 6. SG-Bézier rotation surfaces with the rotation angle θ taking different values. **a** $\theta = 0.5\pi$. **b** $\theta = 1.4\pi$

$\boldsymbol{P}_{i,j}(i = 0, 1, 2, 3;\ j = 1, 2, 3)$ are

$$\boldsymbol{L}^{Z}_{0,j}(s; \lambda_{1,j}, \lambda_{2,j}, \lambda_{3,j}, \omega_j) = \{x_{0,j}(s),\ 0,\ z_{0,j}(s)\}\ \ (0 \le s \le 1, j = 1, 2, 3) \quad (33)$$

where

$$\begin{cases} x_{0,1}(s) = 5 + (3 + \omega_1 - \lambda_{1,1}\omega_1)s + (-12 + 3\lambda_{2,1}\omega_1 + 3\lambda_{1,1}\omega_1 - 12\omega_1)s^2 \\ \quad + (6 - 3\lambda_{1,1}\omega_1 + \lambda_{3,1}\omega_1 - 6\lambda_{2,1}\omega_1 + 22\omega_1)s^3 \\ \quad + (\lambda_{1,1}\omega_1 + \lambda_{3,1}\omega_1 + 3\lambda_{2,1}\omega_1 - 11\omega_1)s^4 \\ z_{0,1}(s) = 13 + (-3 - \omega_1 + \lambda_{1,1}\omega_1)s - (3 - 2\lambda_{2,1}\omega_1 + 3\lambda_{1,1}\omega_1 + 3\omega_1)s^2 \\ \quad + (1 + 3\lambda_{1,1}\omega_1 - 2\lambda_{3,1}\omega_1 - 4\lambda_{2,1}\omega_1 \\ \quad +11\omega_1)s^3 + (-\lambda_{1,1}\omega_1 + 2\lambda_{3,1}\omega_1 + 2\lambda_{2,1}\omega_1 - 7\omega_1)s^4 \\ x_{0,2}(s) = 2 + (-3 - \omega_2 + \lambda_{1,2}\omega_2)s + (6 - 3\lambda_{1,2}\omega_2 - \lambda_{2,2}\omega_2 + 6\omega_2)s^2 \\ \quad + (3\lambda_{1,2}\omega_2 + 3\lambda_{3,2}\omega_2 + 2\lambda_{2,2}\omega_2 \\ \quad - 12\omega_2)s^3 + (-\lambda_{1,2}\omega_2 - 3\lambda_{3,2}\omega_2 - \lambda_{2,2}\omega_2 + 7\omega_2)s^4 \\ z_{0,2}(s) = 8 - (6 + 2\omega_2 - 2\lambda_{1,2}\omega_2)s - (3 + 6\lambda_{1,2}\omega_2 - 3\lambda_{2,2}\omega_2 + 3\omega_2)s^2 \\ \quad + (6\lambda_{1,2}\omega_2 - 4\lambda_{3,2}\omega_2 - 6\lambda_{2,2}\omega_2 \\ \quad +16\omega_2)s^3 + (-2\lambda_{1,2}\omega_2 + 4\lambda_{3,2}\omega_2 + 3\lambda_{2,2}\omega_2 - 11\omega_2)s^4 \\ x_{0,3}(s) = 5 + (9 + 3\omega_3 - 3\lambda_{1,3}\omega_3)s - (18 - 3\lambda_{2,3}\omega_3 - 9\lambda_{1,3}\omega_3 + 18\omega_3)s^2 \\ \quad + (12 - 9\lambda_{1,3}\omega_3 + 3\lambda_{3,3}\omega_3 \\ \quad + 24\omega_3 - 6\lambda_{2,3}\omega_3)s^3 + (3\lambda_{1,3}\omega_3 - 3\lambda_{3,3}\omega_3 + 3\lambda_{2,3}\omega_3 - 9\omega_3)s^4 \\ z_{0,3}(s) = -1 - (12 + 4\omega_3 - 4\lambda_{1,3}\omega_3)s + (4\lambda_{2,3}\omega_3 - 12\lambda_{1,3}\omega_3)s^2 \\ \quad + (3 + 12\lambda_{1,3}\omega_3 - 8\lambda_{2,3}\omega_3 - \lambda_{3,3}\omega_3 \\ \quad +13\omega_3)s^3 + (-4\lambda_{1,3}\omega_3 + \lambda_{3,3}\omega_3 + 4\lambda_{2,3}\omega_3 - 9\omega_3)s^4 \end{cases} \quad (34)$$

here $0 \le \lambda_{1,j}, \lambda_{3,j} \le 4, 0 \le \lambda_{2,j} \le 6,\ 0 \le \omega_j \le 1 (j = 1, 2, 3)$.

In terms of (25), the rotation surface generated by rotating the generating line $\boldsymbol{L}^{Z}_{0,j}(s; \lambda_{1,j}, \lambda_{2,j}, \lambda_{3,j}, \omega_j)$ around the z-axis with one revolution is

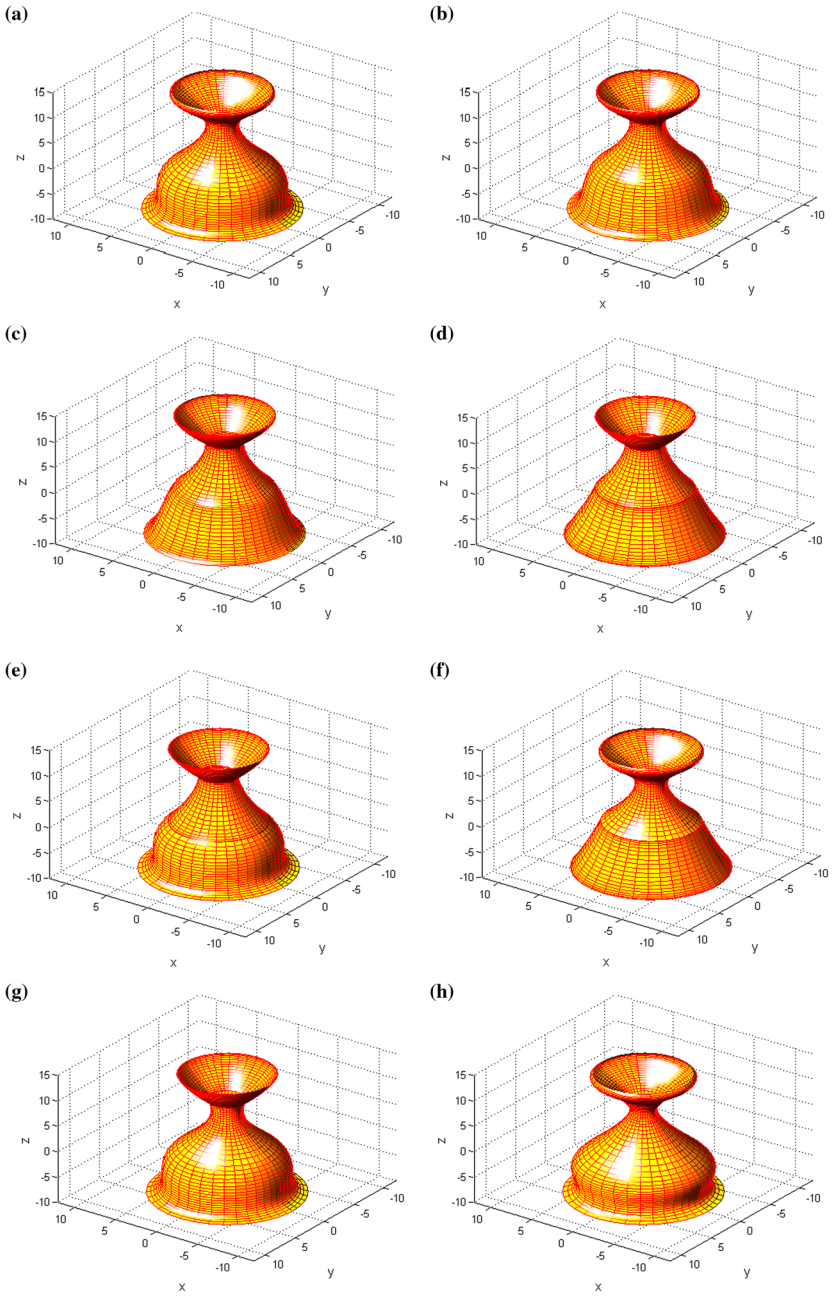
(a)
(b)
(c)
(d)
(e)
(f)
(g)
(h)
x
y
z

◀ FIGURE 7. The composite SG-Bézier rotation surfaces with different shape parameters. **a** $\lambda_{1,j}=4,\lambda_{2,j}=3,\lambda_{3,j}=4;\omega_j=0(j=1,2,3)$. **b** $\lambda_{1,j}=4,\lambda_{2,j}=3,\lambda_{3,j}=4;\omega_j=1/3(j=1,2,3)$. **c** $\lambda_{1,j}=4,\lambda_{2,j}=3,\lambda_{3,j}=4;\omega_j=2/3(j=1,2,3)$. **d** $\lambda_{1,j}=4,\lambda_{2,j}=3,\lambda_{3,j}=4;\omega_j=1(j=1,2,3)$. **e** $\lambda_{1,j}=4,\lambda_{2,j}=3,\lambda_{3,j}=4(j=1,2,3);\omega_1=\omega_2=1,\omega_3=0$. **f** $\lambda_{1,j}=4,\lambda_{2,j}=3,\lambda_{3,j}=4(j=1,2,3);\omega_1=\omega_2=0,\omega_3=1$. **g** $\lambda_{1,1}=4,\lambda_{2,1}=3,\lambda_{3,1}=4,\omega_1=1;\lambda_{1,2}=0,\lambda_{2,2}=0$. **h** $\lambda_{1,1}=0,\lambda_{2,1}=3,\lambda_{3,1}=0,\omega_1=1;\lambda_{1,2}=0,\lambda_{2,2}=6,\lambda_{3,2}=0,\omega_2=1;\lambda_{1,3}=4,\lambda_{2,3}=3,\lambda_{3,3}=4,\omega_3=0\lambda_{3,2}=0,\omega_2=1;\lambda_{1,3}=0,\lambda_{2,3}=6,\lambda_{3,3}=0,\omega_3=1$

$$\begin{cases} \boldsymbol{R}_j^Z(s,t;\lambda_{1,j},\lambda_{2,j},\lambda_{3,j},\omega_j) \\ \quad=\left\{\frac{1-2t}{2t^2-2t+1}x_{0,j}(s),\ \ \frac{2t-2t^2}{2t^2-2t+1}x_{0,j}(s),\ z_{0,j}(s)\right\} \\ \tilde{\boldsymbol{R}}_j^Z(s,t;\lambda_{1,j},\lambda_{2,j},\lambda_{3,j},\omega_j) \\ \quad=\left\{\frac{1-2t}{2t^2-2t+1}x_{0,j}(s),\ \ -\frac{2t-2t^2}{2t^2-2t+1}x_{0,j}(s),\ z_{0,j}(s)\right\} \\ \quad 0\le s,t\le 1, j=1,2,3 \end{cases} \tag{35}$$

where $\boldsymbol{R}_j^Z(s,t;\lambda_{1,j},\lambda_{2,j},\lambda_{3,j},\omega_j)$ and $\tilde{\boldsymbol{R}}_j^Z(s,t;\lambda_{1,j},\lambda_{2,j},\lambda_{3,j},\omega_j)$ constitute a whole rotation surface, and they are symmetrical about the plane xoz; $x_{0,j}(s)$, $z_{0,j}(s)(j=1,2,3)$ can be calculated according to the formulas in (34).

Figure 7 shows graphics of the SG-Bézier rotation surfaces represented by (35) with the shape parameters $\lambda_1,\lambda_2,\lambda_3,\omega$ taking different values, whose generating line represented by (33) is made up of three SG-Bézier curves with G^1 continuity. Thus the whole rotation surface achieves the G^1smooth continuity along the direction of its generating line. As can be seen from Fig. 7, it can be handy, effective and flexible to modify the shape of the composite SG-Bézier rotation surfaces represented by (35) by adjusting its twelve shape control parameters.

5.3. SG-Bézier Rotation Ellipsoid Surfaces

In this section, we give a numerical example of using a SG-Bézier rotation surface to approximately represent an ellipsoid surface (or a sphere surface). In order to facilitate our discussion, given a set of control points $\boldsymbol{P}_j(j=0,1,2,3)$ in the plane xoz whose coordinates are as follows

$$\begin{cases} \boldsymbol{P}_0=(0,\ 0,\ 0) \\ \boldsymbol{P}_1=(1.2,\ 0,\ 0) \\ \boldsymbol{P}_2=(1.2,\ 0,\ 0) \\ \boldsymbol{P}_3=(0,\ 0,\ 2) \end{cases} \tag{36}$$

Then a SG-Bézier curve $\boldsymbol{L}_0^Z(s;\lambda_1,\lambda_2,\lambda_3,\omega)$ can be defined by these control points in (36), which can be used to approximate the semicircle arc $x^2+(z-1)^2=1$ and the semi-elliptical arc $x^2/b^2+(z-1)^2/a^2=1$ $(a=1,0.45\le b\le$

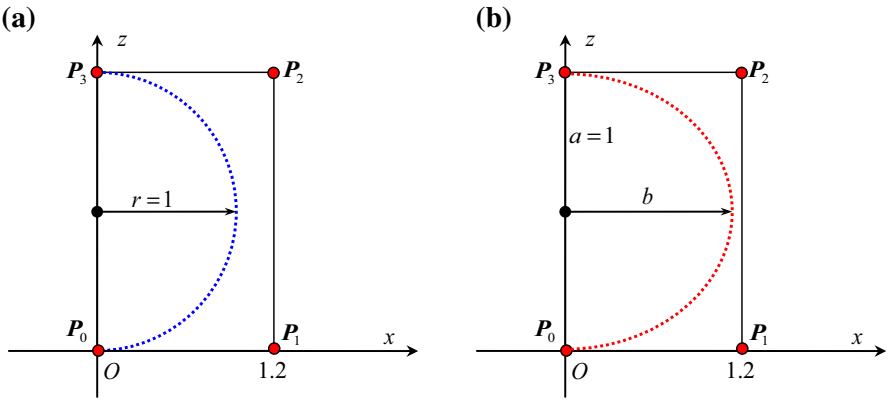

FIGURE 8. Approximation of a semicircle arc and a semi-elliptical arc by using a SG-Bézier curve. **a** Approximation of a semicircle arc. **b** Approximation of a semi-elliptical arc

1.05) as shown in Fig. 8. In this figure, the two black dots are the centers of the circle and ellipse respectively, whose coordinates are fixed as (0, 1), the blue and the red dotted line are the approximated semicircle arc and semi-elliptical arc respectively; the red dots are the four control points of the curve $\boldsymbol{L}_0^Z$. Finally, we can construct a sphere surface or ellipsoid surface by rotating the approximated curve $\boldsymbol{L}_0^Z$ around the z-axis with one revolution. Obviously, how to better approximate the semicircle arc and the semi-elliptical arc is troublesome, so we can adopt the following method: ① Since both semicircle arcs and semi-elliptical arcs are symmetrical curves, the shape adjustable Bézier-like curve $\boldsymbol{L}_0^Z$ need to be symmetrical about the line $z = 1$, combined with the conclusion in 4.4, the parameters should satisfy $\lambda_2 = 3$ and $\lambda_1 = \lambda_3 \neq 1$.② In order to simplify the calculation, we can fix the values of the parameters λ_1, λ_3 and treat the parameter ω as a optimization variable, and then adopt the method in [24] to approximate the semicircle arc $x^2 + (z-1)^2 = 1$ and the semi-elliptical arc $x^2/b^2 + (z-1)^2/a^2 = 1$ by using the curve $\boldsymbol{L}_0^Z(s; \lambda_1^*, 3, \lambda_3^*, \omega)$, where λ_1^*, λ_3^* are constants.

The results calculated by the above method indicate that the curve $\boldsymbol{L}_0^Z(s; 0, 3, 0, 0.671)$ can better approximate the semicircle arc with $\lambda_1 = \lambda_3 = 0$ and $\omega = 0.671$. Finally, we can construct an approximated sphere surface by rotating the curve $\boldsymbol{L}_0^Z(s; 0, 3, 0, 0.671)$ as the generating line around the x-axis with one revolution. In Fig. 9, the yellow curve is the generating line $\boldsymbol{L}_0^Z$ and the blue polygonal line is the control polygon of the generating line.

Similarly, we have: ① When $\lambda_1 = \lambda_3 = 4, \omega = 0.222$, the curve $\boldsymbol{L}_0^Z(s; 4, 3, 4, 0.222)$ can better approximate the semi-elliptical arc $\frac{x^2}{b^2} + \frac{(z-1)^2}{a^2} = 1$ ($a = 1,\ b = 0.8$); ② When $\lambda_1 = \lambda_3 = 4, \omega = 0.667$, the curve $\boldsymbol{L}_0^Z(s; 4, 3, 4, 0.667)$

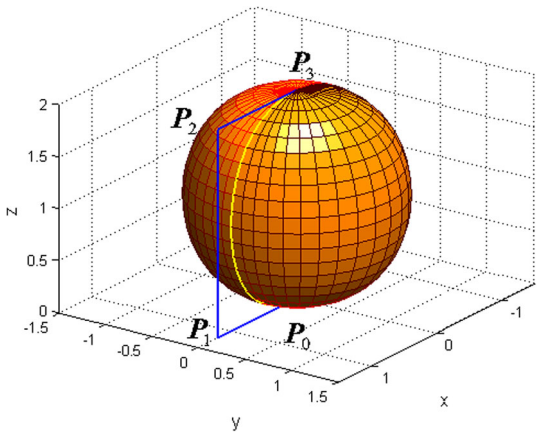

FIGURE 9. Approximation of a sphere surface by using a SG-Bézier rotation surface

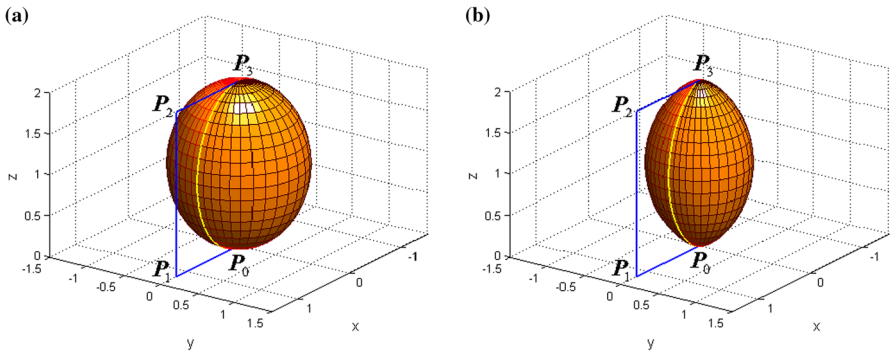

FIGURE 10. The approximation of two ellipsoid surfaces by using a SG-Bézier rotation surface. **a** $a = 1, b = 0.8$. **b** $a = 1, b = 0.6$

can better approximate the semi-elliptical arc $\frac{x^2}{b^2} + \frac{(z-1)^2}{a^2} = 1$ $(a = 1,\ b = 0.6)$. Figure 10 shows the approximation of the generated ellipsoid surfaces in above cases by using a SG-Bézier rotation surface. In Fig. 10a, the generating line of the rotation surface is $\boldsymbol{L}_0^Z(s; 4, 3, 4, 0.222)$, and in Fig. 10b, the generating line of the rotation surface is $\boldsymbol{L}_0^Z(s; 4, 3, 4, 0.222)$.

5.4. SG-Bézier Rotation Ring Surfaces

In this section, we give a numerical example of using a SG-Bézier rotation surface to approximately represent a rotation ring surface. If the control polygon of the SG-Bézier curves is closed, then the curve will also be closed and a rotation ring surface can be constructed by rotating the closed curve as the

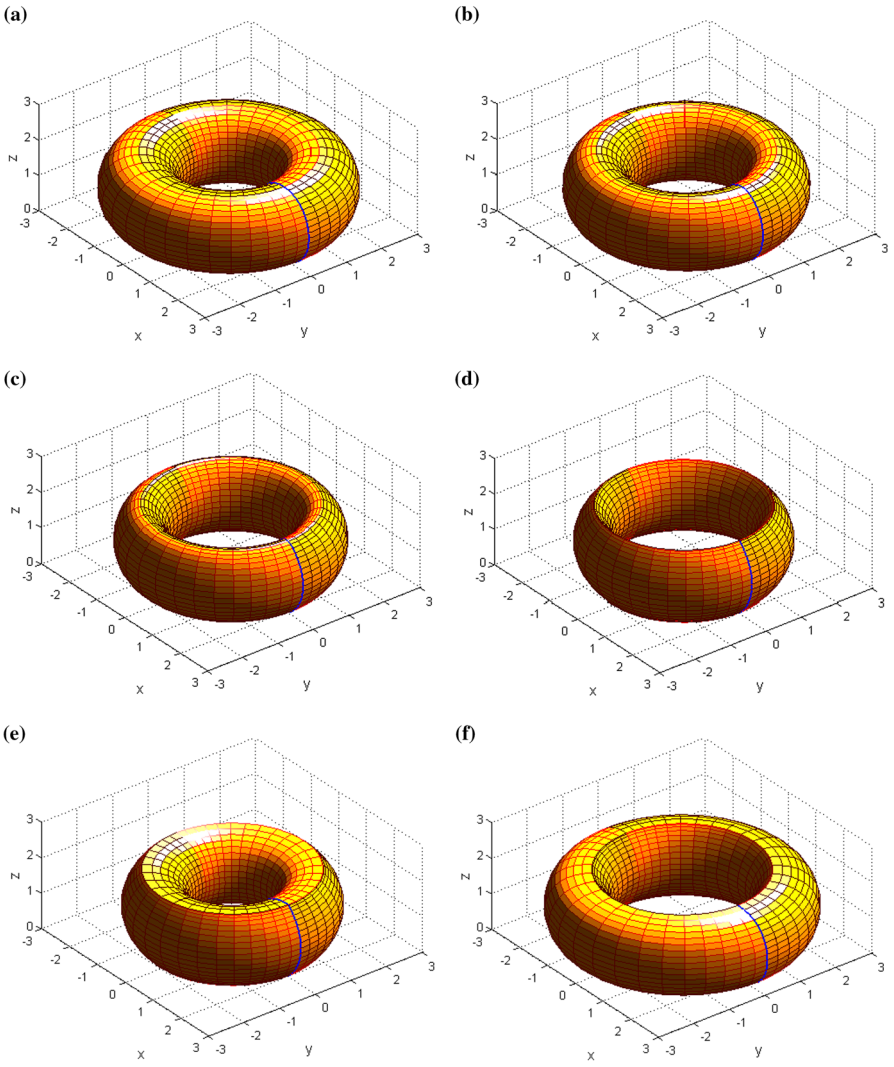

FIGURE 11. SG-Bézier rotating ring surfaces with different shape parameters. **a** $\lambda_{1,j} = 4, \lambda_{2,j} = 3, \lambda_{3,j} = 4; \omega_j = 0 (j = 1, 2)$. **b** $\lambda_{1,j} = 4, \lambda_{2,j} = 3, \lambda_{3,j} = 4; \omega_j = 1/3 (j = 1, 2)$. **c** $\lambda_{1,j} = 4, \lambda_{2,j} = 3, \lambda_{3,j} = 4; \omega_j = 2/3 (j = 1, 2)$. **d** $\lambda_{1,j} = 4, \lambda_{2,j} = 3, \lambda_{3,j} = 4; \omega_j = 1 (j = 1, 2)$. **e** $\lambda_{1,1} = 4, \lambda_{2,1} = 3, \lambda_{3,1} = 4, \omega_1 = 1; \lambda_{1,2} = 0$. **f** $\lambda_{1,1} = 0, \lambda_{2,1} = 3, \lambda_{3,1} = 0, \omega_1 = 1; \lambda_{1,2} = 4, \lambda_{2,2} = 3, \lambda_{3,2} = 0, \omega_2 = 1 \lambda_{2,2} = 3, \lambda_{3,2} = 4, \omega_2 = 1$

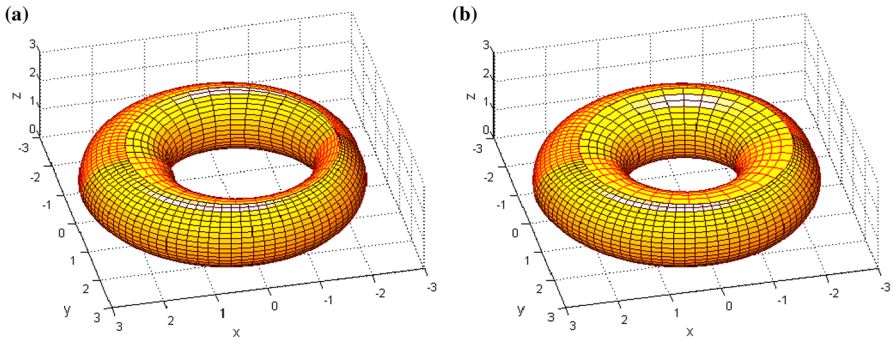

FIGURE 12. The asymmetrical generalized rotation surfaces with transmutative generating line. **a** $\lambda_{1,j}$=4, $\lambda_{2,j}$=3, $\lambda_{3,j}$= 4 (j=1,2). **b** $\lambda_{1,1}$=4,$\lambda_{2,1}$=3, $\lambda_{3,1}$= 4; $\lambda_{1,2}$=0,$\lambda_{2,2}$=3, $\lambda_{3,2}$= 0

generating line around a rotation axis with one revolution. In order to facilitate our discussion, given a set of control points $\boldsymbol{P}_{i,j}(i = 0, 1, 2, 3;\ j = 1, 2)$ in the plane xoz whose coordinates are as follows

$$\begin{cases} \boldsymbol{P}_{0,1} = (2,\ 0,\ 0), \boldsymbol{P}_{1,1} = (3.2,\ 0,\ 0) \\ \boldsymbol{P}_{2,1} = (3.2,\ 0,\ 2), \boldsymbol{P}_{3,1} = (2,\ 0,\ 2) \\ \boldsymbol{P}_{0,2} = (2,\ 0,\ 0), \boldsymbol{P}_{1,2} = (0.8,\ 0,\ 0) \\ \boldsymbol{P}_{2,2} = (0.8,\ 0,\ 2), \boldsymbol{P}_{3,2} = (2,\ 0,\ 2) \end{cases} \tag{37}$$

Then we can construct a closed SG-Bézier curve $\boldsymbol{L}^Z_{0,j}(s; \lambda_{1,j}, \lambda_{2,j}, \lambda_{3,j}, \omega_j)(j = 1, 2)$ and obtain the rotation surface generated by rotating $\boldsymbol{L}^Z_{0,j}$ as the generating line around the z-axis with one revolution according to (25).

$$\begin{cases} \boldsymbol{R}^Z_j(s,t;\lambda_{1,j},\lambda_{2,j},\lambda_{3,j},\omega_j) = \left\{ \frac{1-2t}{2t^2-2t+1}x_{0,j}(s),\ \ \frac{2t-2t^2}{2t^2-2t+1}x_{0,j}(s),\ z_{0,j}(s) \right\} \\ \tilde{\boldsymbol{R}}^Z_j(s,t;\lambda_{1,j},\lambda_{2,j},\lambda_{3,j},\omega_j) = \left\{ \frac{1-2t}{2t^2-2t+1}x_{0,j}(s),\ \ -\frac{2t-2t^2}{2t^2-2t+1}x_{0,j}(s),\ z_{0,j}(s) \right\} \end{cases} \tag{38}$$

where $0 \le s,t \le 1, 0 \le \lambda_{1,j}, \lambda_{3,j} \le 4, 0 \le \lambda_{2,j} \le 6,\ 0 \le \omega_j \le 1 (j = 1, 2)$; $\boldsymbol{R}^Z_j(s,t)$ and $\tilde{\boldsymbol{R}}^Z_j(s,t)$ constitute a whole rotation ring surface, and the calculating formulas for $x_{0,j}(s), z_{0,j}(s)(j = 1, 2)$ are as follows

$$\begin{cases} x_{0,1}(s) = 2 + (\frac{18}{5} + \frac{6}{5}\omega_1 - \frac{6}{5}\lambda_{1,1}\omega_1)s - (\frac{18}{5} - \frac{18}{5}\lambda_{1,1}\omega_1 + \frac{18}{5}\omega_1)s^2 \\ \quad + (\frac{24}{5}\omega_1 - \frac{18}{5}\lambda_{1,1}\omega_1 - \frac{6}{5}\omega_1\lambda_{3,1})s^3 + (\frac{6}{5}\lambda_{1,1}\omega_1 + \frac{6}{5}\lambda_{3,1}\omega_1 - \frac{12}{5}\omega_1)s^4 \\ z_{0,1}(s) = (-6 - 6\omega_1 + 2\lambda_{2,1}\omega_1)s^2 + (4 + 12\omega_1 - 4\lambda_{2,1}\omega_1)s^3 \\ \quad + (2\lambda_{2,1}\omega_1 - 6\omega_1)s^4 \\ x_{0,2}(s) = 2 - (\frac{18}{5} + \frac{6}{5}\omega_2 - \frac{6}{5}\lambda_{1,2}\omega_2)s + (\frac{18}{5} - \frac{18}{5}\lambda_{1,2}\omega_2 + \frac{18}{5}\omega_2)s^2 \\ \quad - (\frac{24}{5}\omega_2 - \frac{18}{5}\lambda_{1,2}\omega_2 - \frac{6}{5}\omega_2\lambda_{3,2})s^3 - (\frac{6}{5}\lambda_{1,2}\omega_2 + \frac{6}{5}\lambda_{3,2}\omega_2 - \frac{12}{5}\omega_2)s^4 \\ z_{0,2}(s) = (-6 - 6\omega_2 + 2\lambda_{2,2}\omega_2)s^2 + (4 + 12\omega_2 - 4\lambda_{2,2}\omega_2)s^3 \\ \quad + (2\lambda_{2,2}\omega_2 - 6\omega_2)s^4 \end{cases} \tag{39}$$

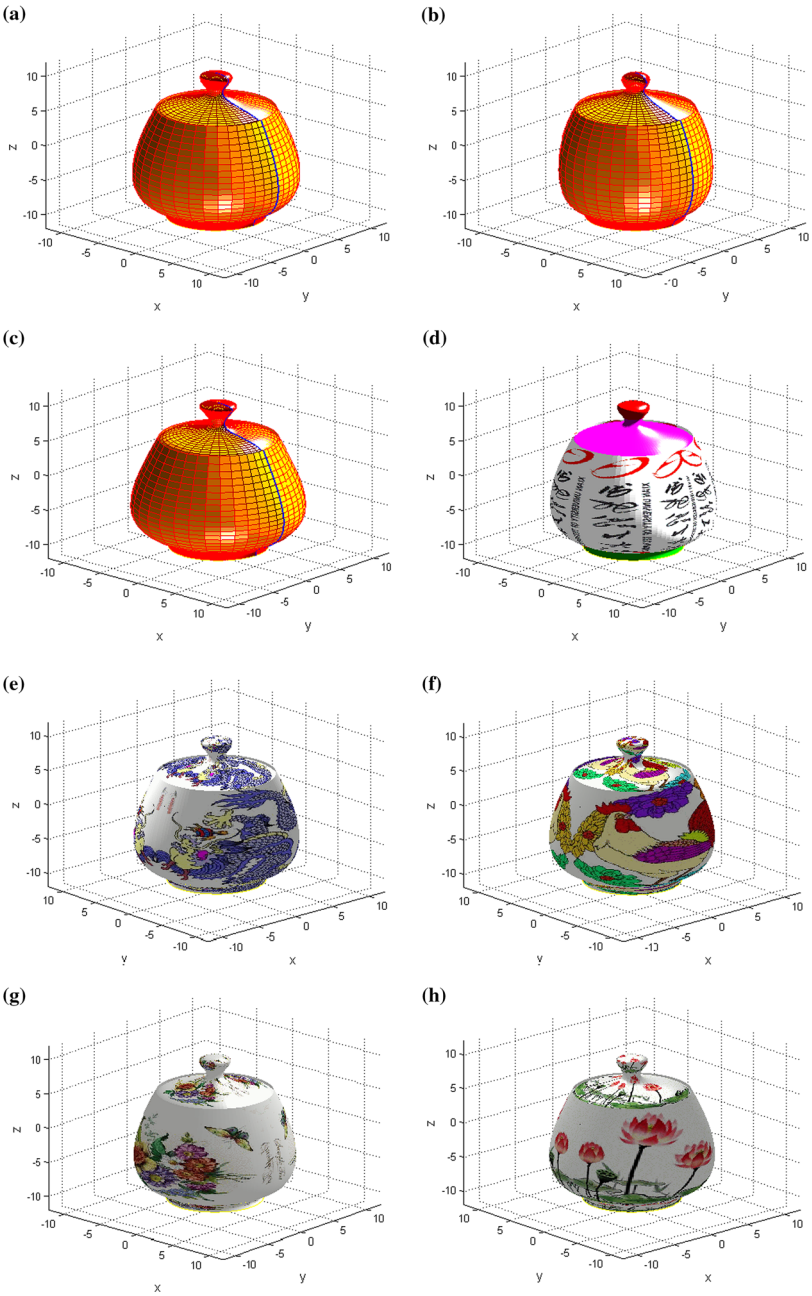
(a)
(b)
(c)
(d)
(e)
(f)
(g)
(h)
x
y
z

◀ FIGURE 13. Designing rotation surface graphs of rounded ceramic pot. **a** Original rotation surfaces. **b** Deformed rotation surfaces-1. **c** Deformed rotation surfaces-2. **d** Texture mapping surface. **e** Colored drawing surface-1. **f** Colored drawing surface-2. **g** Colored drawing surface-3. **h** Colored drawing surface-4 (color figure online)

Figure 11 shows some graphics of the SG-Bézier rotation ring surfaces in (38) with different shape parameters. In this figure, the blue curve is the generating line of the rotation ring surface, which is a closed curve composed of two SG-Bézier curves. Obviously, the shape of the rotation ring surface can be modified handily by adjusting its eight shape control parameters, reducing both time and effort.

5.5. Asymmetrical Generalized Rotation Surfaces with Transmutative Generating Line

For a traditional rotation surface, its generating line will not deform in the process of rotation, making the surface is symmetrical about its rotation axis. Such as the rotation surfaces in [3–19] (except for [10]) and the SG-Bézier rotation surfaces in this paper. A rotation surface whose generating line deforms in the process of rotation is called a generalized rotation surface, which is asymmetrical [10]. The following discussion is focused on how to use the SG-Bézier curves to generate this kind of asymmetrical generalized rotation surface, and the concrete approach is as follows: since the generating line $\tilde{\boldsymbol{L}}_0 : \boldsymbol{L}_{0,j}(s;\lambda_{1,j},\lambda_{2,j},\lambda_{3,j},\omega_j)(j = 1,2,\ldots,n)$ of the SG-Bézier rotation surfaces contains four different shape parameters $\lambda_{1,j},\lambda_{2,j},\lambda_{3,j},\omega_j$, the generating line could modify its shape in the process of rotation, thus generating a asymmetrical generalized rotation surface with the generating line deforming. For instance, fixing the values of the parameters $\lambda_{1,j},\lambda_{2,j},\lambda_{3,j}$, an asymmetrical generalized rotation surface can be constructed by modifying the value of the parameter ω_j of the generating line $\tilde{\boldsymbol{L}}_0$ in the process of rotation. In order to facilitate our discussion, the parameters $\lambda_{1,j},\lambda_{2,j},\lambda_{3,j}$ and ω_j are called the shape control parameters and the generatrix deforming parameter of the generalized rotation surface respectively. It should be noted that the distinction of the two kinds of parameters is, the shape control parameters need to be given before the asymmetrical generalized rotation surface is constructed; while the generatrix deforming parameter is not a constant any more, but a variable of the rotation surface. Figure 12 gives a numerical example to show graphics of an asymmetrical generalized rotation surface with its generating line deforming. In Fig. 12, the control points of the generating line $\tilde{\boldsymbol{L}}_0$ of the asymmetrical generalized rotation surfaces are the same as those in Fig. 11; ω_j and $\lambda_{1,j},\lambda_{2,j},\lambda_{3,j}(j = 1,2)$ are the generatrix deforming parameter and shape control parameters of the asymmetrical generalized rotation surfaces respectively.

6. Applications

As an extension of classic Bézier rotation surfaces, the SG-Bézier rotation surfaces provide a new class of mathematical theory for the development of CAD/CAM application software, and its application range includes manufacturing industry, computer graphics, computer vision, computer animation, multimedia technology, etc. In CAD/CAM, if the apparent surface of a product is a complex rotation surface, the surface need to be considered as a piecewise rotation surface composed of multiple ones. Figure 13 gives an example to design the rotation surface of rounded ceramic pot. In this figure, the blue curve is the generatrix of the rotation surface, which is composed of four SG-Bézier curves.

In recent years, how to realize the 3D modeling and rendering of ancient buildings by using computer technology has always been a research hot topic in computer graphics, game software development and digital preservation of cultural heritage sites and objects, etc. Ancient Hakka earthen buildings are a unique architectural style in ancient Chinese buildings with their construction having some significant geometric features, such as the Hall of Prayer for Good

Harvest in Beijing's Temple of Heaven. Figure 14 gives an example to design the rotation surface of rounded Ancient Hakka earthen building by using the proposed method in this paper. In this figure, the generatrix of the rotation surface is composed of ten SG-Bézier curves, each of which satisfies G^0 or G^1 continuity with its adjacent one.

7. Conclusions

In order to tackle the problem that the shape of a traditional rotation surface often can not be modified expediently, we present a method to construct a new kind of SG-Bézier rotation surfaces in this paper based on the basic idea of BTVRI function. Furthermore, we analyze the properties of this kind of rotation surfaces and discuss the influence rules of their shape parameters. The SG-Bézier rotation surfaces possess the following advantages: ① They inherit the outstanding properties of the traditional Bézier rotation surfaces, but their shape adjustability is superior to that of the traditional Bézier rotation surfaces. So without redefining the generating line, the local or global shape of a SG-Bézier rotation surface can be modified handily only by adjusting its shape parameters; ② We introduce multiple shape parameters in the construction of the rotation surfaces, which increases the flexibility in rotation surface design and overcomes the problem that the shape of a traditional rotation surface often can not be modified expediently; ③ They possess their explicit function expression, making the coordinate of any point on the surface can be easily got and the speed of generating rotation surfaces raised. In this paper, the theoretical analysis and modeling examples show that the method for generating SG-Bézier rotation surfaces is intuitive and easy to implement. Furthermore,

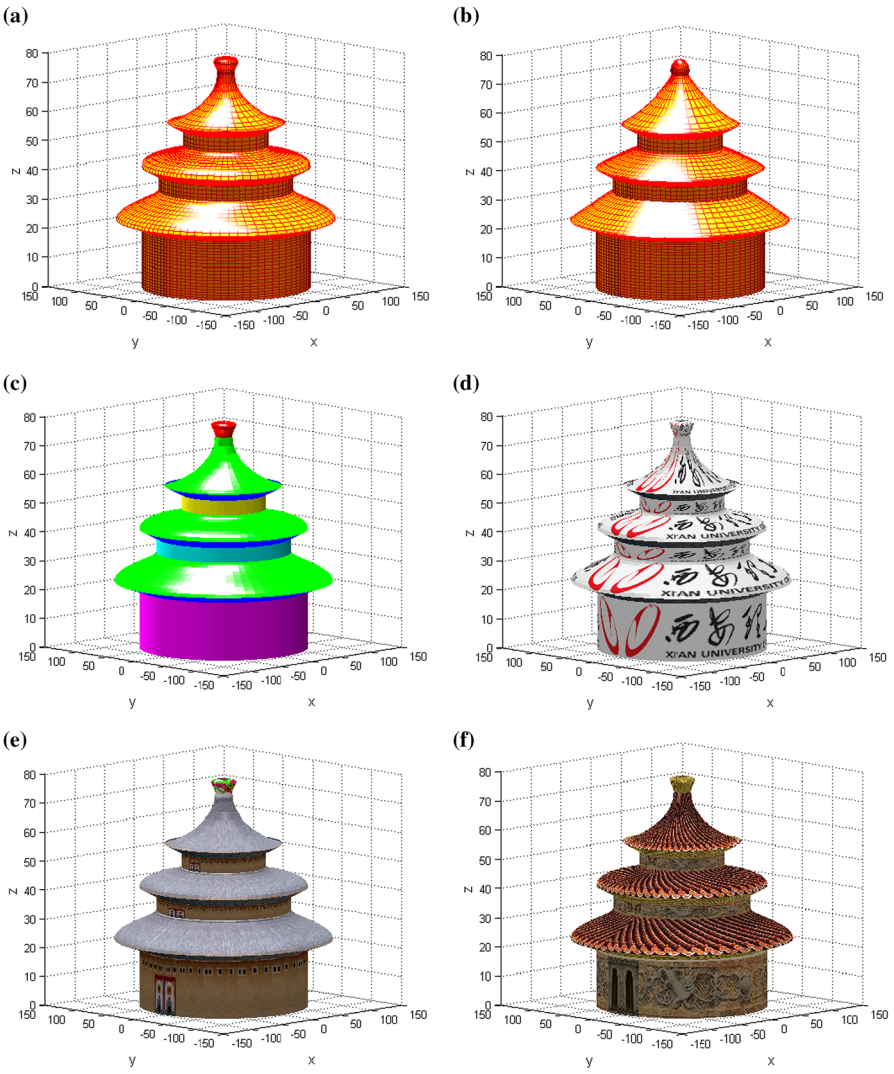

FIGURE 14. Rotational surface modeling of ancient Hakka earthen buildings. **a** Original rotation surfaces. **b** Deformed rotation surfaces. **c** Colored lighting surface. **d** Texture mapping surface. **e** Colored drawing surface-1. **f** Colored drawing surface-2 (color figure online)

the proposed method provides appearance shaping design of rotation surfaces with additional degrees of freedom. Thus they can be used to construct complex surfaces of revolution with different degrees of smoothness. We will focus on studying the problem of how to construct a SG-Bézier rotation surface with

minimal bending energy in future work. In addition, how to apply the proposed method to 3-D reconstruction and modeling of complex rotation surfaces in reverse engineering is worthy for further study.

Acknowledgements

This work is supported by the National Natural Science Foundation of China (Nos. 51305344, 11501443, 11626185). This work is also supported by the Research Fund of Shaanxi, China (No. 2014K05-22).

References

[1] Piegl, L., Tiller, W.: The NURBS Book, 2nd edn. Springer, New York (1997)

[2] Farin, G.: Curves and Surfaces for CAGD: A Practical Guide, 5th edn. Academic Press, San Diego (2002)

[3] Farin, G., Piper, B., Worsey, A.: The octant of a sphere as a non-degenerate triangular Bézier patch. Comput. Aided Geom. Des. **4**(4), 329–332 (1987)

[4] Wang, G.J.: A new method for representing the surface of revolution using rational B-splines in CAD. J. Softw. **1**(4), 24–39 (1990)

[5] Kang, B.S., Ma, X., Zhou, R.R.: On the representation of revolution surface and sphere by NURBS polynomial. J. Nanjing Univ. Aeronaut. Astronaut. **26**(1), 80–87 (1994)

[6] Zeng, T.J., Wang, W.M., Zhang, J.W.: Study on surfaces of revolution modeling with C-B-splines. J. Graph. **25**(2), 104–108 (2004)

[7] Ma, S.J., Liu, X.M.: Research of rotate surface of uniform T-B-spline. Comput. Eng. Des. **29**(16), 4255–4256 (2008)

[8] Ding, H., Zhu, L.M.: Geometric Theories and Methods for Digital Manufacturing of Complex Surfaces. Science Press, Beijing (2011)

[9] Bourguignon, D., Cani, M.P., Drettakis, G.: Drawing for illustration and annotation in 3D. Comput. Graph. Forum **20**(3), 114–122 (2001)

[10] Dai, C.L., Ding, Y.L., Lu, X.: On generalized revolving surface based on metamorphose curve. Mech. Sci. Technol. **21**(4), 537–539 (2002)

[11] Rodrigues, A.B., Jorge, J.A.: Free form modeling with variational implicit surfaces. In: Proceedings of the 12th Encontro Português de Computacao Gráfica, pp.17–26. Porto, Portugal (2003)

[12] Wong, K.Y.K., Mendonca, P.R.S., Cipolla, R.: Reconstruction of surfaces of revolution from single uncalibrated views. Image Vis. Comput. **22**(10), 829–836 (2004)

[13] Colombo, C., Bimbo, A.D., Pernici, F.: Metric 3D reconstruction and texture acquisition of surfaces of revolution from a single uncalibrated view. IEEE Trans. Pattern Anal. **27**(1), 99–114 (2005)

[14] Wu, Y.H., Wang, G.H., Wu, F.C., Hu, Z.Y.: Euclidean reconstruction of a circular truncated cone only from its uncalibrated contours. Image Vis. Comput. **24**(8), 810–818 (2006)

[15] Li, X.J., Liu, H., He, G., Liao, W.: Generation and shape adjustment of revolution surface based on stream curve. Mech. Sci. Technol. **27**(3), 326–329 (2008)

[16] Han, L., Raffaele, D.A.: Rotation surface modeling technique by cubic B-spline free drawing. J. Chin. Comput. Syst. **30**(7), 1141–1144 (2009)

[17] Gong, X.P., Li, M.Z., Lu, Q.P., Peng, Z.Q.: Continuous forming for rotary surface based on multi-point adjusting principle. Opt. Precis. Eng. **20**(1), 117–123 (2012)

[18] Wang, Y., Fang, M.: Non-homogeneous subdivision method of revolution surfaces based on generalized B-spline. J. Hangzhou Dianzi Univ. **33**(2), 25–28 (2013)

[19] Lionel, G., Hichem, B., Sebti, F.: Dupin cyclide blends between non-natural quadrics of revolution and concrete shape modeling applications. Comput. Graph. **42**(1), 31–41 (2014)

[20] Tan, J.Q.: Continued Fractions Theory and its Application. Science Press, Beijing (2007)

[21] Gu, C.Q.: Bivariate Thiele-type matrix-valued rational interpolants. J. Comput. Appl. Math. **80**(1), 71–82 (1997)

[22] Tan, J.Q., Tang, S.: Bivariate composite vector valued interpolation. Math. Comput. **69**(232), 1521–1532 (2000)

[23] Zhu, X.L.: A new method for constructing circular arc. J. Hefei Univ. Technol. **25**(2), 269–272 (2002)

[24] Kim, S.H., Ahn, Y.J.: An approximation of circular arcs by quartic Bézier curves. Comput. Aided Des. **39**(6), 490–493 (2007)

Gang Hu and Junli Wu
Department of Applied Mathematics
Xi'an University of Technology
Xi'an 710054
People's Republic of China
e-mail: hg_xaut@xaut.edu.cn

Gang Hu
School of Mechanical and Precision Instrument Engineering
Xi'an University of Technology
Xi'an
People's Republic of China

Guo Wei
University of North Carolina at Pembroke
Pembroke, NC, 28372
USA

Received: August 18, 2016.
Accepted: February 14, 2017.